

# Geochemistry, Geophysics, Geosystems



## RESEARCH ARTICLE

10.1029/2020GC009333

### Key Points:

- Rocks recovered from the Mar del Plata Canyon area, 38°S in the Western South Atlantic, are interpreted as ice-rafted debris
- Antarctic Peninsula, sub-Antarctic islands in the Scotia Sea and Tierra del Fuego are identified as plausible source areas
- Dropstones lie as a coarse sediment drape inside morphological depressions

### Supporting Information:

- Supporting Information S1

### Correspondence to:

G. Bozzano,  
[grazi.hidro.gov.ar@gmail.com](mailto:grazi.hidro.gov.ar@gmail.com);  
[gbozzano@hidro.gov.ar](mailto:gbozzano@hidro.gov.ar)

### Citation:







Bozzano, G., Cerredo, M. E., Remesal, M., Steinmann, L., Hanebuth, T. J. J., Schwenk, T., et al. (2021). Dropstones in the Mar del Plata Canyon area (SW Atlantic): Evidence for provenance, transport, distribution, and oceanographic implications. *Geochemistry, Geophysics, Geosystems*, 22, e2020GC009333. <https://doi.org/10.1029/2020GC009333>

Received 31 JUL 2020  
 Accepted 8 DEC 2020

© 2020. The Authors.

This is an open access article under the terms of the Creative Commons Attribution-NonCommercial-NoDerivs License, which permits use and distribution in any medium, provided the original work is properly cited, the use is non-commercial and no modifications or adaptations are made.

## Dropstones in the Mar del Plata Canyon Area (SW Atlantic): Evidence for Provenance, Transport, Distribution, and Oceanographic Implications

G. Bozzano<sup>1,2</sup> , M. E. Cerredo<sup>3</sup>, M. Remesal<sup>3</sup>, L. Steinmann<sup>4</sup>, T. J. J. Hanebuth<sup>5</sup> , T. Schwenk<sup>4</sup> , M. Baqués<sup>1,6</sup> , D. Hebbeln<sup>7</sup> , D. Spoltore<sup>1</sup>, O. Silvestri<sup>1,8</sup>, R. D. Acevedo<sup>9,10</sup>, V. Spiess<sup>4</sup>, R. A. Violante<sup>1</sup>, and S. Kasten<sup>4,7,11</sup> 

<sup>1</sup>Department of Oceanography, Argentine Hydrographic Service (SHN), Buenos Aires, Argentina, <sup>2</sup>CONICET, Buenos Aires, Argentina, <sup>3</sup>IGeBA (UBA-CONICET), University of Buenos Aires, Buenos Aires, Argentina, <sup>4</sup>Faculty of Geosciences, University of Bremen, Bremen, Germany, <sup>5</sup>Department of Coastal and Marine Systems Science, Coastal Carolina University, South Carolina, SC, USA, <sup>6</sup>Argentine Navy Research Office (DIIV), UNIDEF, Buenos Aires, Argentina, <sup>7</sup>MARUM – Center for Marine Environmental Sciences, University of Bremen, Bremen, Germany, <sup>8</sup>DCAO, Faculty of Exact and Natural Sciences, University of Buenos Aires, Buenos Aires, Argentina, <sup>9</sup>Centro Austral de Investigaciones Científicas (CADIC-CONICET), Ushuaia, Argentina, <sup>10</sup>Universidad Nacional de Tierra del Fuego, (ICPA-UNTDF), Ushuaia, Argentina, <sup>11</sup>Alfred Wegener Institute Helmholtz Centre for Polar and Marine Research, Bremerhaven, Germany

**Abstract** A variety of gravel- to cobble-sized rocks, recovered from the Mar del Plata (MdP) Canyon area (Western South Atlantic at 38°S) and interpreted as ice-rafted debris, represent the first evidence that large icebergs have floated in the Falkland (Malvinas) Current from the southern polar high latitudes far northward. Detailed petrographic analyses identified the Antarctic Peninsula, sub-Antarctic islands in the Scotia Sea, and Tierra del Fuego as plausible source areas. The drift process could have started as early as at the beginning of the last deglaciation, according to an age obtained from a cold-water coral fragment associated with one of the dropstones. At the end of the Last Glacial Maximum, large icebergs have been supplied to the Antarctic Circumpolar Current, captured by those ocean current branches that circumvent the Falkland (Malvinas) Islands and entered the Argentine Margin. When the iceberg fleets approached the Brazil-Falkland (Malvinas) Confluence Zone with its steep latitudinal temperature gradient, the icebergs got oceanographically trapped and melted off rapidly. The sediment load sinking down to the seafloor formed a dropstone blanket particularly where the MdP Canyon had incised into the continental slope. Here, mass-flow processes, induced by local slope instability, and along-slope sediment resorting, due to the erosional effects of strong and persistent contouritic bottom currents, favored local enrichment in dropstones in the form of a loose, coarse sediment drape inside morphological depressions. The bottom current velocity would be locally strong enough to rework this sediment, leaving coarse rafted debris as a lag deposit.

**Plain Language Summary** Icebergs can transport sand- to cobble-sized sediment while drifting with the ocean currents over large distances away from the high latitudes. When seawater temperature forces the ice to melt, this “ice-rafted debris” will sink down as “dropstones” to the seabed. Offshore dropstone deposits are common in polar regions but rarely found in lower latitudes because icebergs barely survive if the ocean water is not extremely cold. We found evidence of dropstone deposits along the Argentine Margin at the relatively low latitude of 38°S. They rest inside morphological seafloor depressions at the continental slope in association with the Mar del Plata Canyon. Here, also the oceanic Brazil-Falkland (Malvinas) Confluence Zone is located, which acts as a barrier for northward drifting icebergs. The presence of icebergs in the Argentine Sea was already known; we, however, describe the first finding of rocks that clearly had originated from the Antarctic Peninsula, sub-Antarctic islands in the Scotia Sea, and Tierra del Fuego, the southern tip of the South American continent. These dropstones are often found together with fragments of cold-water corals, suggesting that the imported rocks have locally served as hard substrate for coral colonies to establish.

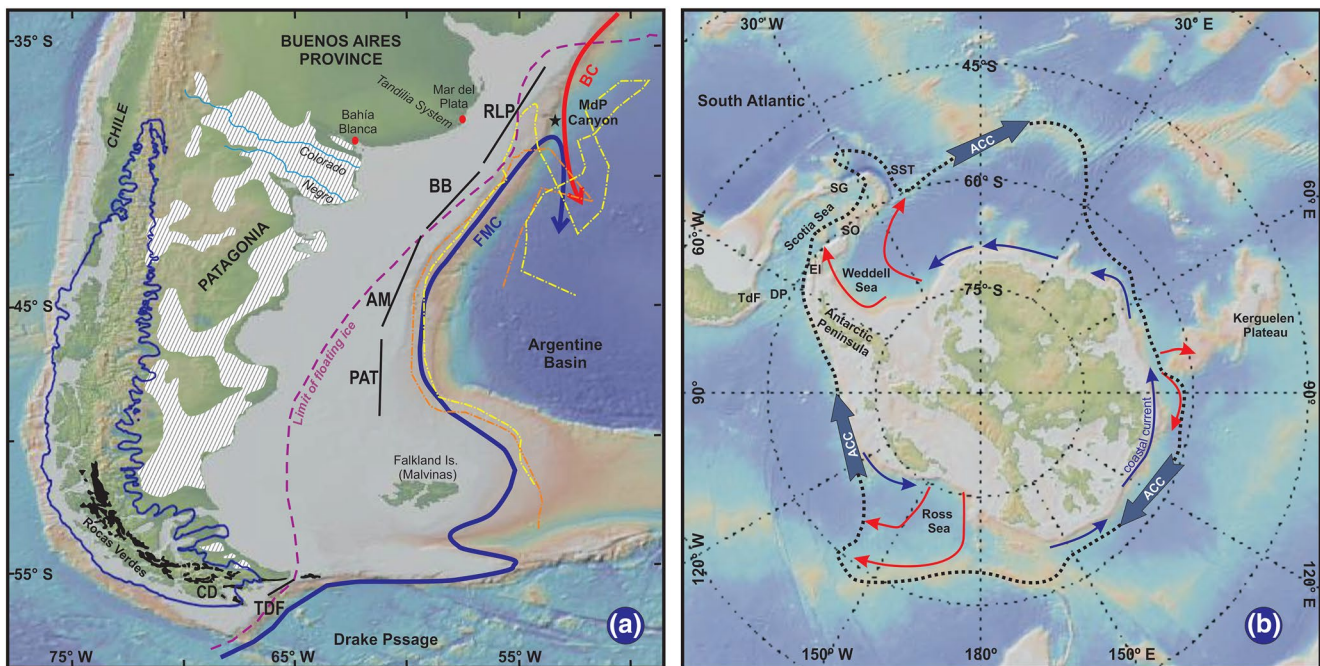


**Figure 1.** The Argentine Continental Margin and the Southern Ocean. (a) Location of the Mar del Plata (MdP) Canyon study area (black star). The Patagonian Ice Sheet extent at 35 ka (Davies et al., 2020) is indicated by a blue line. The patchy distribution of the gravel-rich units known as “Rodados Patagónicos” is shown by shaded areas (Martínez et al., 2009). Argentine Submarine Canyon Systems. The trajectories of two Argo floats (yellow and orange lines), deployed at 53.07°S and 54.29°W, followed the FMC along the 1,000-m isobath up to the latitude of 38°S (from Artana et al., 2018). Icebergs have historically been observed east of the limit of floating ice (SHN Chart H5011, 2002). (b) The Antarctic region. Iceberg trajectories in the Antarctic Coastal Current are indicated by black arrows; icebergs detaching from the coast at the Ross Sea, Kerguelen Plateau, and the Weddell Sea are depicted by red arrows (after Gladstone et al., 2001; Rackow et al., 2017; Schodlok et al., 2006). Figure base map from GeoMapApp, <http://www.geomapapp.org>. ACC, Antarctic Circumpolar Current (Orsi et al., 1995); AM, Ameghino; BB, Bahía Blanca; BC, Brazil Current; CD, Cordillera Darwin; DP, Drake Passage; EI, Elephant Island; FMC, Falkland (Malvinas) Current; PAT, Patagonia; RLP, Río de la Plata; SG: South Georgia Island; SO: South Orkney Island; SST: South Sandwich Trench; TdF, Tierra del Fuego.

## 1. Introduction

Dropstones are defined as single, exotic clasts of anomalous size and lithology from remote sources, indicative of a vertical supply into the host sediment (Bennett et al., 1996). They may drop down from melting sea ice or be reworked from a parent glaciomarine deposit. Dropstones and ice-rafted debris (IRD) in marine sediments have been largely studied because they provide valuable information on ice sheet growth and decay dynamics as well as global sea-level variability and oceanographic change (Weber et al., 2018).

Dropstones have frequently been reported from both the northern and southern hemispheres, particularly from areas located close to glaciated margins. At the Argentine Continental Margin (ACM), dropstones of various size and petrography have been described by several authors (Bornhold, 1983; Conolly & Ewing, 1965; Goodell, 1964; Plafker et al., 1977). They have been observed for the first time at the seafloor in the Drake Passage, Scotia Sea, and South Sandwich Trench (Figure 1; Goodell, 1964). Subsequent studies have concluded that the occurrence of IRD extends as far north as the Falkland (Malvinas) Plateau (50°S latitude), that Antarctica would be the most likely source area, and that the rafting happened at least since the late Miocene and all through the Cenozoic (Bornhold, 1983; Ciesielski et al., 1982; Plafker et al., 1977). More recently, detailed morpho-bathymetric surveys have reported plough marks and iceberg scours at 50°S in the Northern Falkland (Malvinas) Basin (Brown et al., 2017) and, at 45°S at the Patagonian continental margin (López-Martínez et al., 2011), the latter being the northernmost morphological evidence for giant icebergs routing the South Atlantic so far. The presence of icebergs drifting in the Argentine Sea in modern times is not unknown to sailors who have historically reported occasional icebergs up to the latitudes off Uruguay and Southern Brazil (Figure 1a). In 2002, a 700 × 100 m sized iceberg was spotted 120 miles off Mar del Plata (MdP), traveling north-northeastward at a speed of 1.7 km/h (La Nación, 2002). Nevertheless,

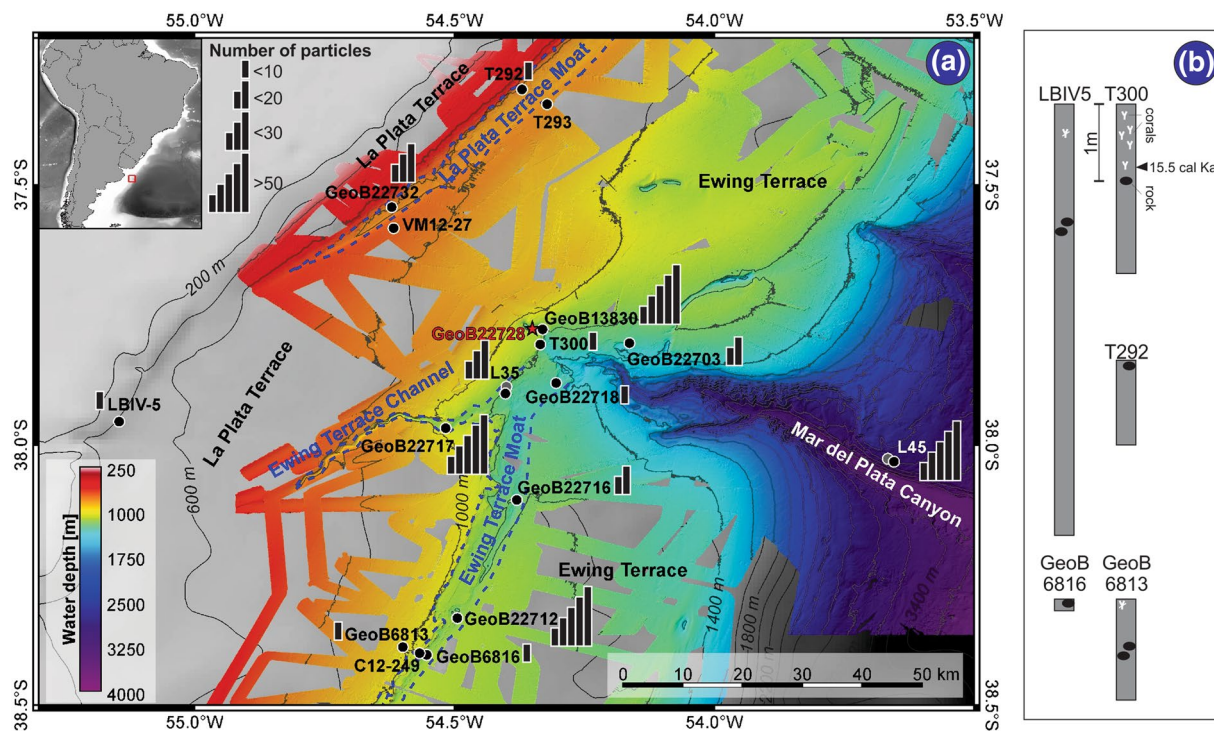


**Figure 2.** The study area and rock distribution. (a) Bathymetric map of the Mar del Plata Canyon area with the sites used in the study. Dashed blue lines follow the main path of La Plata Terrace Moat, Ewing Terrace Channel and Ewing Terrace Moat. Sites GeoB from the Bremen University, Sites LB and T from the Argentine Hydrographic Service, Sites L from the Argentine Natural Science Museum Bernardino Rivadavia, VM and C stand for Sites Vema and Conrad available from GeoMapApp Data Base. CTD casts at Sites GeoB22718 and GeoB22728. Rock distribution is shown by frequency bars. (b) Schematic representation of the gravity cores collected in the study area where pebbles were obtained.

no geological evidence has yet confirmed that icebergs together with their IRD load have reached the latitude of MdP (38°S).

In this study, we present the analysis of pebble and cobble deposits from modern water depths ranging from 600 to 2,900 m in proximity to the MdP Canyon, particularly from the head area, one deep-sea channel, two contouritic moats, and surrounding slope locations. This study pursued the following objectives: (1) to determine the petrography of the retrieved pebbles and cobbles with the aim to identify their probable source regions; (2) to find evidence for the regional transport mechanisms that control the material distribution; and (3) to understand the local sedimentary processes that favored the concentration of this material at specific sites in the wider MdP Canyon area. We demonstrate that the large amount of coarse IRD in the MdP Canyon area corresponds to the instability of the Antarctic Ice Sheets at the beginning of the last deglaciation and, having accumulated in local morphological depressions, results from the combination of regional paleo-climatic and oceanographic configurations in interplay with local erosional and sedimentary processes.

## 2. Regional Setting

The ACM extends from the Río de la Plata estuary in the north (36°S) to the Scotia Sea in the south (57°30'S; Figure 1). Five major submarine canyon systems incise into the continental slope: Río de la Plata, Bahía Blanca, Ameghino, Patagonian, and Tierra del Fuego (Bozzano et al., 2017; Hernández-Molina et al., 2009; Lonardi & Ewing, 1971; Figure 1a). The margin is also shaped by a huge Contourite Depositional System composed of a complex suite of erosive (e.g., furrows, moats, channels, terraces) and depositional (e.g., plastered, elongated and detached drifts) elements (Hernández-Molina et al., 2009). MdP Canyon, the largest of the Río de la Plata Canyon System (Lonardi & Ewing, 1971), is located in the northern sector of the margin more than 250 km off the coast (Figure 2a). Here, the continental slope can be differentiated into

upper (150–700 m), middle (700–1,300 m), and lower sectors (1,300–3,500 m modern water depth; Violante et al., 2010). The MdP Canyon starts at the middle slope (also referred to as Ewing Terrace) at 900 m water depth and opens at 3,900 m, where the lower slope turns into the continental rise (Krstel et al., 2011). According to the conceptual model for canyon systems proposed by Harris and Whiteway (2011), this canyon has been classified as slope-confined (Bozzano et al., 2017), since no connection to the shelf exists. The main canyon valley runs sinuous in its upper course and relatively straight and deeply incised in its lower (Bozzano et al., 2017; Warratz et al., 2019). The MdP Canyon is fed by tributary channels that have been partially mapped (Figure 2a; Krstel et al., 2011; Preu et al., 2013; Steinmann et al., 2020; Warratz et al., 2019). Some of these deep-sea channels, mainly running parallel to the isobaths, have been interpreted as being of contouritic origin (Hernández-Molina et al., 2009; Preu et al., 2013; Violante et al., 2017), meaning that they were carved in by lasting and strong contour-parallel bottom currents. One of the most developed channels was recently defined as a contourite moat and named Ewing Terrace Moat (Steinmann et al., 2020). In contrast, other channels show an oblique or downslope orientation, and seem to be more associated with downslope sedimentary processes or contour-normal, near-bottom oceanographic forcing elements (Figure 2a).

The oceanic circulation at the ACM is dominated by the northward-flowing, cold and nutrient-rich Falkland (Malvinas) Current (FMC), originating in the Drake Passage from the northernmost branch of the Antarctic Circumpolar Current (ACC; Piola & Gordon, 1989). The vertical distribution of the intermediate-to-bottom water masses includes Antarctic Intermediate Water (AAIW; ~500–1,000 m water depth), Circumpolar Deep Water (CDW; ~1,000–3,500 m) and Antarctic Bottom Water (AABW; > 3,500 m). North Atlantic Deep Water (NADW) penetrates into the CDW from the north and divides it into Upper (UCDW) and Lower CDW (LCDW; Tsuchiya et al., 1994). Roughly within the latitudinal range of 35°–45°S (Garcia, 2004), the FMC collides with the southward-flowing Brazil Current (BC; Figure 1a), which represents the western limb of the South Atlantic subtropical gyre that transports warm and saline waters in poleward direction. The encounter of these two western boundary currents results in a joint seaward directed deflection that is referred to as the Brazil-Falkland (Malvinas) Confluence Zone, which is accompanied by a complex pattern of meanders and cold and warm-core eddies formation (Gordon, 1989). Here, both temporal and local changes in surface temperature (7°C–24°C) and salinity (30.0–36.0) are considerably frequent and abrupt.

### 3. Materials and Methods

Multibeam bathymetric and hydro-acoustic surveying of the MdP Canyon region was performed during RV Meteor cruise M78/3a in 2009 (Krstel et al., 2011) and during RV Sonne cruise SO260/1 in 2018 (Kasten et al., 2019). While the former expedition used a Kongsberg EM120 echosounder, the latter cruise obtained improved lateral morphological resolution of the canyon and adjacent deep-sea channels using a Kongsberg EM122 system; both systems operated at a frequency of 12 kHz. Subbottom profiles were collected with a parametric sediment echosounder (Atlas PARASOUND P700) during both cruises with a parametric signal frequency of 4 kHz that provides a very-high vertical resolution of a few decimeters (Steinmann et al., 2020). During cruise SO260/1, the hull mounted Ocean Surveyor Teledyne RDI Acoustic Doppler Current Profiler (ADCP) with a doppler shift of 38 kHz provided real-time current velocity profiles over a range from 38 to 1,200 m water depth. ADCP data from the lowest 10%–15% of the water column have been removed due to possible scattering caused by strong seafloor echo. Doppler shifts were converted into current velocities using real water sound velocities by means of Conductivity-Temperature-Depth (CTD) and Expendable Sound Velocimeter profile calibration. A Sea-Bird SBE 9.11 CTD profiler equipped with sensors for temperature, conductivity, pressure (PSA 916), oxygen (SBE 43), and altimeter was employed during cruise SO260/1 (Kasten et al., 2019).

Sediment and rock samples from the MdP Canyon head area, deep-sea channel, contourite moats, and adjacent slope were collected with various devices (box corer, Van Veen grab, trawling dredge, gravity, and piston corers) during a number of successive expeditions (Meteor M78/3a, Cañón Submarino II/III, Litoral Bonaerense IV, Coring 2002, Sonne SO260/1, Figure 2, Table 1). Often, solely rock material was received by these devices as the finer sediment fraction was lost during the retrieval due to rock fragments hindering the complete closure of the sampling device. If recovered, the rock-hosting sediment was wet-sieved over 4 and 2 mm sieves. Fraction  $\phi > 4$  mm (pebbles and cobbles) was separated for petrographic analysis; fraction

**Table 1**

*List and Position of the Geological Samples Used in this Study for Sediment Grain Size and/or Dropstone Petrographic Determination*

Name	Cruise	Latitude, °S	Longitude, °W	Water depth (M)	Location (sampler)
Canyon head					
GeoB13830-1	M78/3a	37°46.66	54°19.83	1262	(BC)
T300	Coring 2002	37°48.4	54°20.1	1300	(PC)
La Plata Terrace Moat					
GeoB22732-1	SO260/1	37°32.567	54°37.236	798	(G)
T292	Coring 2002	37°19.0	54°22.2	870	(PC)
T293	Coring 2002	37°20.7	54°19.3	860	(PC)
VM12-27	Vema	37°35.0	54°37.02	745	(PC)
Ewing Terrace Channel					
GeoB22717-1	SO260/1	37°58.047	54°31.007	1165	(G)
Ewing Terrace Moat					
GeoB22712-3	SO260/1	38°19.953	54°29.665	1214	(BC)
GeoB22716-1	SO260/1	38°06.329	54°22.803	1287	(G)
GeoB22718-1	SO260/1	37°52.846	54°18.263	1411	(G)
GeoB6813-1	M49/2	38°23.29	54°35.96	985	(GC)
GeoB6816-1	M49/2	38°24.20	54°33.20	1180	(GC)
C12-249	Conrad	38°24.0	54°34.02	1196	(PC)
Other samples from the continental slope					
GeoB22703-1	SO260/1	37°48.252	54°09.805	1320	(BC)
L35	Cañón Submarino II/III	37°54.06 (start) 37°53.28 (end)	54°24.12 (start) 54°24.0 (end)	1245 (start) 1220 (end)	(TD)
L45	Cañón Submarino II/III	38°1.913 (start) 38°1.586 (end)	53°39.268 (start) 53°39.972 (end)	2,934 (start) 2,952 (end)	(TD)
LBIV-5	LB IV	37°57.3	55°08.7	616	(PC)

BC, Box-corer; G, Van Veen grab; GC, Gravity corer; PC, Piston corer; TD, Trawling Dredge.

*Note.* Sampler.

4 > Ø > 2 mm (granules) was studied under a binocular for qualitative inspection of the sediment composition; and fraction Ø < 2 mm was analyzed for grain size distribution with a CILAS 1190 laser particle size analyzer, covering a range between 0.04 and 2,500 µm. All pebbles and cobbles were macroscopically described and classified in broad lithologic groups (sedimentary, metamorphic, and igneous). A few rock samples were selected as representative and 36 thin sections were prepared for microscopic determination of their mineralogical composition. In addition, a fragment of a cold-water coral (CWC) found in core T300 close to a pebble (Figure 2b) was dated by Uranium-series dating at the Institute for Environmental Physics at the Heidelberg University (IUP), Germany, according to the procedure described in Frank et al. (2004) and recently updated by Wefing et al. (2017).

## 4. Results

### 4.1. Seafloor Morphology and Surface Sediment Grain Size

#### 4.1.1. Canyon Head Area

The canyon head area, where Site GeoB13830 is located, displays an E-W trending 150-m deep and 1.3-km wide channel that abruptly changes its course into N-S direction (Figure 3). Core GeoB13830-1 was obtained from the channel floor, which is constrained by steep sidewalls (13°–30°) with CWC mounds at the top of the southern flank. Almost 3 km apart, Core T300 was retrieved from the southern flank of a CWC

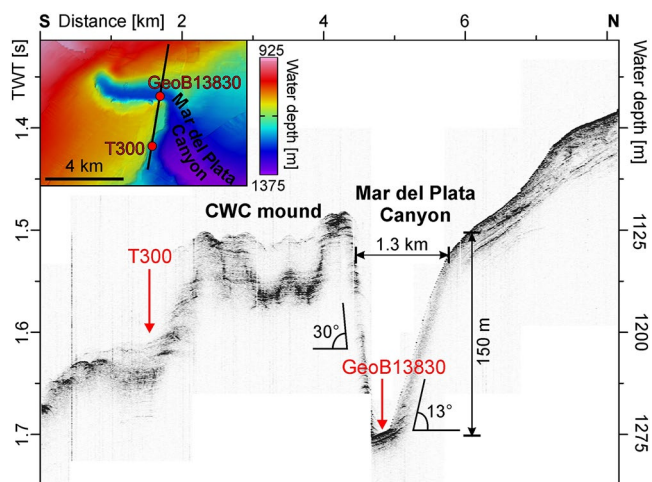


**Figure 3.** Cross-section of the Mar del Plata Canyon head area at the location of Sites T300 and GeoB13830, which are separated one from each other by cold-water coral (CWC) mounds. Upper left corner: detailed bathymetric map of the canyon head area showing the position of the seismic cross-section.

mound. A coral fragment found at 84 cm sediment depth in this core has been dated to  $15.5 \pm 0.25$  cal ka BP (Figure 2b). The surface sediment, inferred from the analysis of the core tops GeoB13830-1 and T300, is composed of fine sand with a mixture of terrigenous material (mostly quartz, feldspars, glass shards, lithic fragments) and planktonic foraminifera.

#### 4.1.2. Deep-Sea Channel and Contouritic Moats

One deep-sea channel and two contouritic moats were identified in the MdP Canyon area (Figure 2a). The La Plata Terrace Moat is located north of the MdP Canyon on the La Plata Terrace, that is, at the transition between upper and middle slope at a water depth of  $\sim 700$ – $800$  m. It is aligned along a SW-NE direction parallel to the isobaths, with a length of 35 km from Site VM12-27 to Site T293. At Site GeoB22732, the 2-km wide thalweg is confined to the northwest by a  $>90$ -m high,  $17^\circ$ -steep scarp, which was eroded into the subparallel-layered strata (Figure 4a). To the southeast, La Plata Terrace Moat is bounded by a 65-m thick mounded drift of a more gentle ( $<3^\circ$ ) dip and well-stratified internal packages (Figure 4a). At Site VM12-27, the moat is deeply entrenched between a  $>100$ -m high scarp to the northwest and a 94-m thick and up to  $5^\circ$ -steep mounded drift to the southeast. Here, the 1.5-km wide thalweg is partly covered by a chaotic, hummocky acoustic facies dipping to the east that might correspond to mass-wasting deposits, which are detached from the

steep scarp (Figure 4b). The surface sediment, inferred from the analysis of Grab GeoB22732-1, is composed of fine sand ( $\phi_{\text{mean}} 135 \mu\text{m}$ ; percentages of sand-silt-clay 58-30-12), with the coarsest fraction reaching  $600 \mu\text{m}$  in diameter (Figure S1). These results are consistent with previous analyzes at the neighboring Sites T292 and T293 (Bozzano et al., 2011) and VM12-27 (GeoMapApp database at <http://www.geomapp.org>).

The Ewing Terrace Channel is situated on the Ewing Terrace south of the MdP Canyon, at the middle continental slope at water depths of 800–1,200 m (Figure 2a). Its entrance shows an oblique WSW-ENE direc-

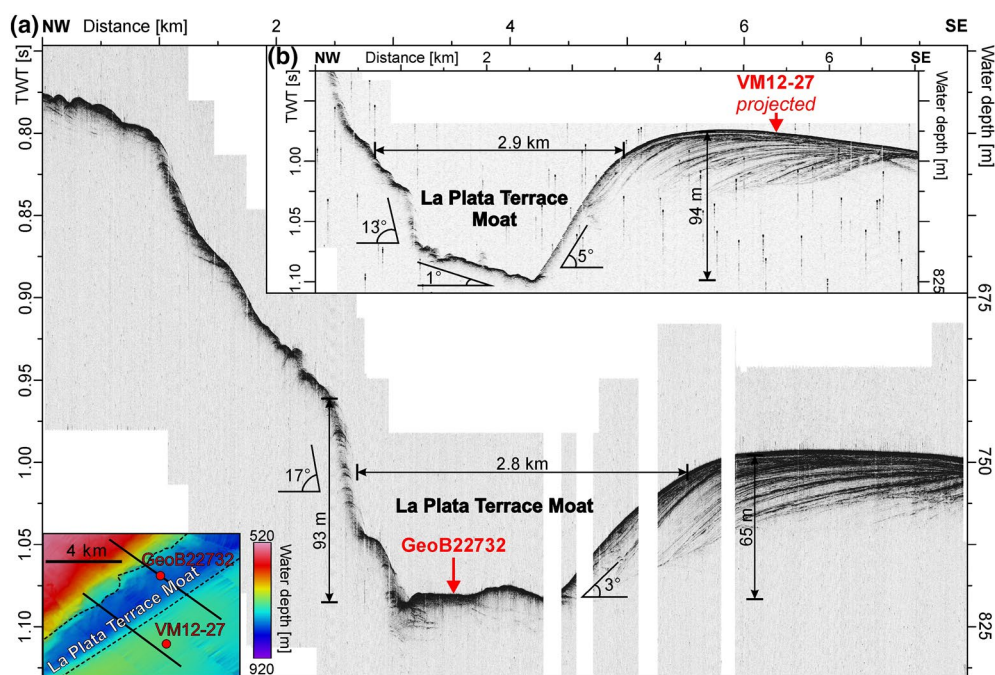


**Figure 4.** Cross-sections of La Plata Terrace Moat at the location of Sites (a) GeoB22732 and (b) VM12-27. The height and the slope angle of the moat walls are indicated, as well as the width of the moat. Lower left corner: detailed bathymetric map of La Plata Terrace Moat where the two seismic cross-sections are located.

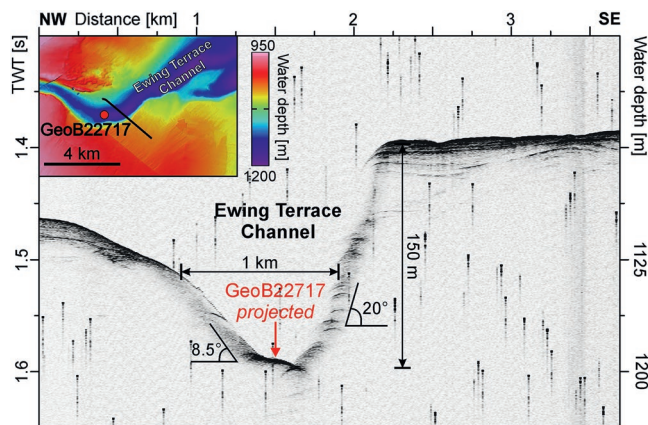


**Figure 5.** Cross-section of the Ewing Terrace Channel next to the location of Site GeoB22717. The height and the slope angle of the south-eastern channel wall are indicated, as well as the width of the channel floor. Upper left corner: detailed bathymetric map of Ewing Terrace Channel showing the position of the seismic cross-section.

tion, and the channel turns into a more across-slope NW-SE orientation, before merging with the Ewing Terrace Moat and jointly entering the MdP Canyon. The channel path is sinuous and the thalweg is deeply entrenched at Site GeoB22717 (Figure 5). The surface sediment, embedding large pebbles, and cobbles retrieved in Grab GeoB22717-1, are composed of medium silt ( $\phi_{\text{mean}} 20 \mu\text{m}$ ; percentages of sand-silt-clay 5-72-23). A small coarse fraction is constituted of very fine sand, with  $112 \mu\text{m}$  as the coarsest grain size found (Figure S1).

The Ewing Terrace Moat was developed along the Ewing Terrace south of MdP Canyon at water depths of 1,000–1,100 m following an along-slope SW-NE direction, at a length of 50 km from Site C12-249 to Site GeoB22718. The thalweg, which progressively widens while the moat reaches the MdP Canyon (Figure 2a), is deeply entrenched in-between more than 100-m high and  $13^{\circ}$ – $35^{\circ}$ -steep sidewalls (Figure 6; see also detailed description in Steinmann et al., 2020). Site GeoB22718 is located in a morphological depression of the moat close to the MdP Canyon, 1.3 km wide, with a small mounded drift developed on the east-south-eastern side (Figure 6a). At Site GeoB22716 (further south), the moat is entrenched into  $9^{\circ}$ – $16^{\circ}$ -steep and 68–100-m high sidewalls (Figure 6b).

At Site GeoB22712, the southernmost site in the moat, the thalweg is 700 m wide; the west-northwestern sidewall of the moat was carved into sub-parallel-oriented strata and displays a step-like morphology, each step ranging 25–30 m in height (Figure 6c). The seafloor inside the moat is covered by fine sand ( $\phi_{\text{mean}} 170 \mu\text{m}$ ; percentages of sand-silt-clay at the top of Core GeoB6816-1 75-20-5), with a coarsest grain size of  $600 \mu\text{m}$  (Figure S1). These results with high proportions (60%–70%) of sand are similar to the previously reported neighboring Site RC12-249 (GeoMapApp database at <http://www.geomapp.org>).

#### 4.1.3. Continental Slope North of the Canyon

Two examples from the continental slope, at the northern side of the MdP Canyon, are portrayed in Figure 7. At 1,300 m water depth (Ewing Terrace, Site GeoB22703), the bathymetry displays a depression with two topographic steps at its northeastern flank, which are 70 and 35 m high, respectively, and carved into subparallel-stratified older geological formations. It is associated with a 40-m elevating, plastered drift that is located at the lower topographic step (Figure 7a). At about 3,000 m water depth (Site L45), the lower continental slope at the edge of the canyon is characterized by a hummocky, chaotic acoustic facies, which is comparable to a mass-wasting deposit that is located at the exit of a small, downslope-directed incision (Figure 2a). Along the NW-SE trending profile shown in Figure 7b, which runs parallel to the canyon wall, this deposit is > 12 km in lateral elongation and > 300 m high.

#### 4.2. Rock Samples: Size, Surface Morphology, Petrography, and Geographic Distribution

The rocks retrieved from the MdP Canyon head area, Ewing Terrace Moat and Channel, La Plata Terrace Moat and adjacent continental slope form a poorly sorted population of lithoclasts, covering a wide range in grain size from granules to small cobbles, with large and very large pebbles as the predominant class (16–64 mm in diameter). Rock surface morphology is variable, including some specimens of high surface relief, angular to subangular shape, or rough surface. Others have a moderate relief, subrounded to rounded shape, with scattered vugs, and faceted surfaces (Figure 8a). Lithoclasts of rounded to oblate shape and with a polished surface, sometimes showing grooves and pits, are also present (Figure 8b). Numerous rocks show a platy shape, an angular or flatiron shape, broken edges, and abrasional facets; striae and stoss-lee forms are occasionally observed (Figures 8b and 8c). These characteristics are, in this combination, typical features of glacially eroded material.

Detailed rock petrography was analyzed on 36 selected rocks. Igneous (16) and sedimentary rocks (12) dominate the assemblage, whereas metamorphic rocks (8) are less represented. Among the igneous rocks, more volcanic (13) than intrusive (3) lithologies were identified. Very fine grained volcanoclastic rocks,

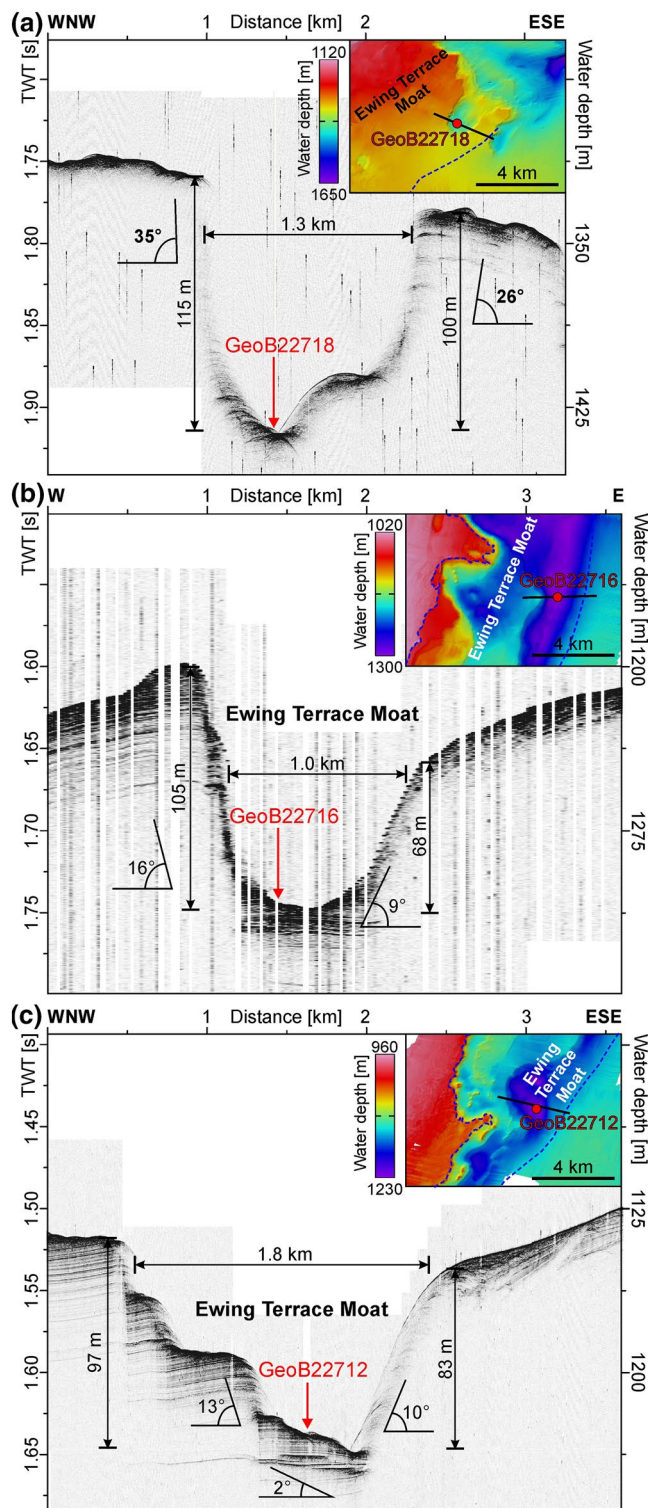


**Figure 6.** Cross-sections of the Ewing Terrace Moat at the location of Sites GeoB22718 (a), 22716 (b), and 22712 (c). For each site, the detailed bathymetric map of the moat is shown on the upper right corner.

rich in sharp-edged volcanic rock fragments, glass shards, and pumiceous material are frequent. The volcanic rocks cover a wide spectrum from acidic (rhyolite), to intermediate (rhyodacite, andesite) and basic composition (olivine basalt). The intrusive rock types (sienogranite, granodiorite, and tonalite) show some degree of incipient deformation such as undulating optical extinction in quartz grains, mechanically oriented crystals, and brittle deformation. Sedimentary rocks include calcareous sandstones, greenish to dark gray, very fine to medium grained sandstones, and yellowish wackestones and greywackes. These latter types of rocks often contain glass shards, pumiceous fragments, and glauconite as minor components. The metamorphic rocks can be divided into three groups according to their grade of metamorphism and protolith nature. Metasedimentary rocks include garnet-bearing granulite and biotite-sillimanite schist, both indicating a high metamorphic degree, and three fine-grained schist specimens that reflect a medium grade metamorphic history. Finally, three samples were classified as metavolcanic rocks, of which two have an acidic and one a basic composition.

The geographic distribution of this rock population is described in detail in the following according to each investigated site location (Figure 2; Table 1). When recovered with Van Veen grabs or trawling dredges, it is assumed that rocks rested at the very surface on the seafloor. When recovered with box, piston, or gravity corer, the particular depth, at which rocks were found, is specified in relation to the seafloor.

#### 4.2.1. Canyon Head Area

Box core GeoB13830-1, 1,262 m water depth. A large number of rocks ranging from gravel up to large cobble (250 mm in diameter) was found at a sediment depth interval of 4–22 cm. The detailed petrographic analyses, performed on 14 of these rocks, showed a great lithological diversity. Sedimentary (greenish-gray greywackes, yellowish micritic wackestones, calcareous, lithic and Qtz-rich sandstones) and igneous rocks (andesite, basaltic andesite, granodiorite, tonalite, and very fine-grained tuffs) are equally abundant. One metamorphic rock was determined as a garnet-bearing granulite.

#### 4.2.2. La Plata Terrace Moat

Grab GeoB22732-1, 798 m water depth. Rocks with grain sizes ranging from large pebbles (16–32 mm) to cobbles (115 mm) included sandstones, conglomerates, granites, volcanic, and metamorphic rocks; other small pebbles of not further identified lithology had a polished surface. The grain surfaces of 40% of this assemblage were faceted. Corals, worm tubes, and mollusk fragments were abundant.

Piston core T292, 860 m water depth. Two small-to-medium sized pebbles of volcanic origin (rhyolite/rhyodacite and trachybasalt) were found at 2–3 cm core depth within a finer matrix and interpreted as contouritic gravel-rich facies (Bozzano et al., 2011).

#### 4.2.3. Ewing Terrace Channel

Grab GeoB22717-1, 1,165 m water depth. Large pebble (16–32 mm) up to cobble (90 mm) sized rocks consisted of light-brown sandstones, igneous (mostly granitoids and rhyolite), and metamorphic lithology. One diagnostic metamorphic rock displayed internal banding with Q and M do-



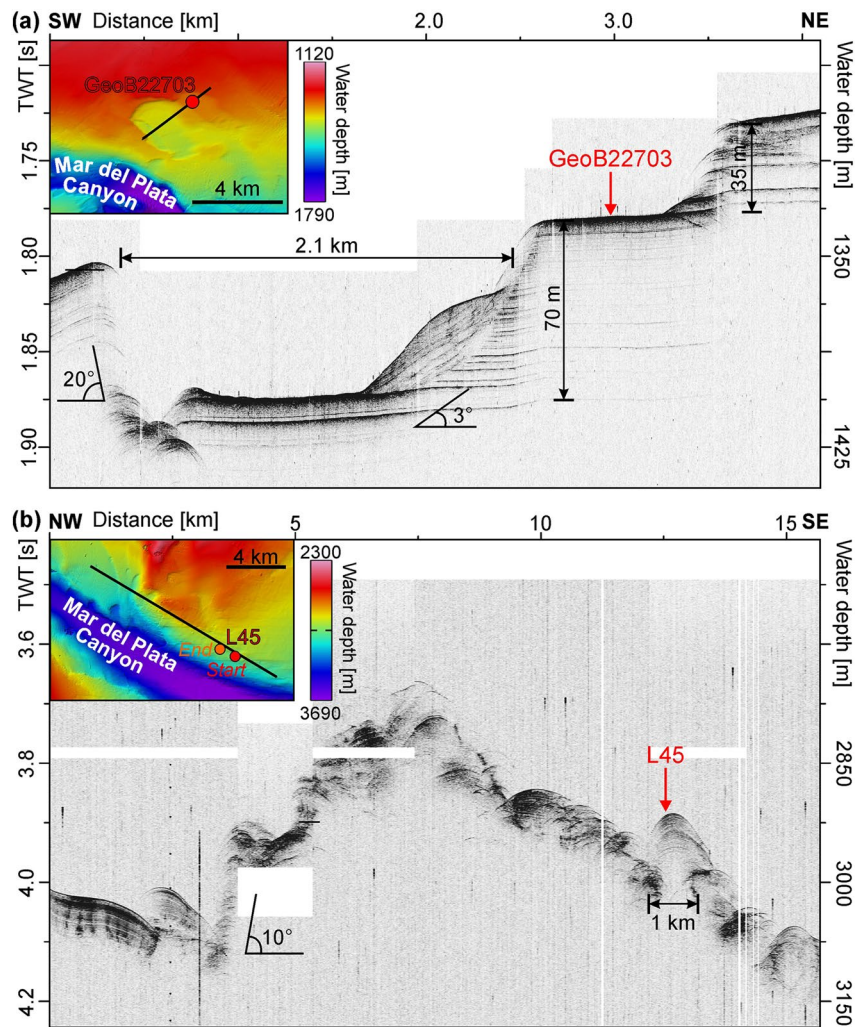


**Figure 7.** (a) Cross-section of the Ewing Terrace, north of Mdp Canyon, at the location of Site GeoB22703 where the most outstanding features are the step-like morphology of the slope carving into subparallel-stratified older geological formations and the plastered drift occupying the lower topographic step; (b) cross-section of the lower continental slope, north of Mdp Canyon, at the location of Site L45 showing a chaotic seismic facies comparable to a mass-wasting deposit. For each site, the detailed bathymetric map showing the position of the seismic cross-section is portrayed on the upper left corner.

mains, composed of a fine grained (0.2–0.3 mm) granoblastic quartz > feldspar aggregates and biotite-muscovite interlayering with a very high aspect ratio. Bundles of sillimanite needles, scarce tourmaline crystals and zircon inclusions in biotite complete the metamorphic assemblage (Figures 9a–9c). Half of the material from this site showed faceted surfaces.

#### 4.2.4. Ewing Terrace Moat

Box core GeoB22712-3, 1,214 m water depth. Numerous medium pebble (8–16 mm) up to cobble sized (82 mm) specimens were obtained from the sub-seafloor. They were immersed in loose, medium to coarse sandy sediment, and associated with coral fragments (Kasten et al., 2019). Sedimentary rocks, forming more than half of the assemblage, were mostly composed of yellowish micritic wackestones showing abundant lithic fragments of volcanic origin, pumice, glass shards, glauconite, and mineral-replaced organic remains (Figures 9d–9e). The igneous group was composed by pinkish or grayish granitoids, acidic and basic volcanic rocks, and various volcanoclastic specimens. Metamorphic rocks ranged from gneiss to fine-grained

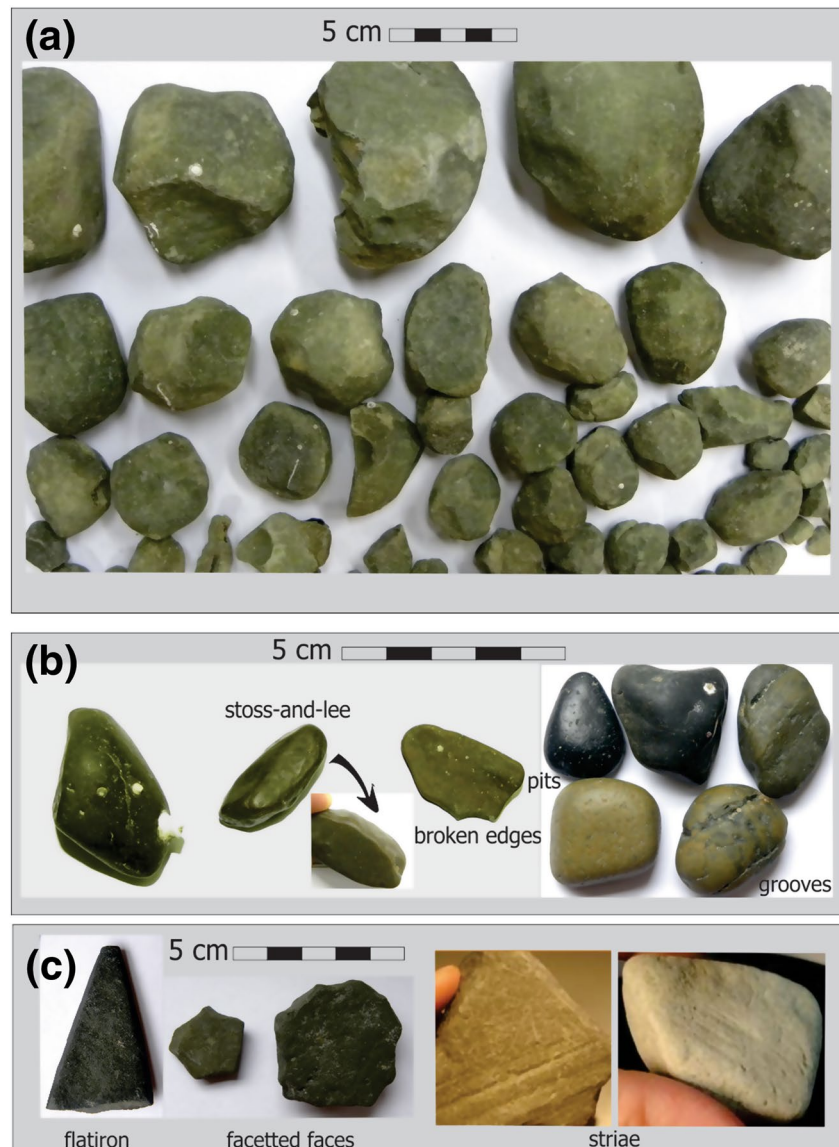


**Figure 8.** Rock morphology. (a) Pebbles from Site GeoB22712 (Ewing Terrace Moat) with subangular to subrounded, equant shape, moderate to high relief and faceted faces in most cases. (b) Pebbles from Site GeoB22712 (Ewing Terrace Moat; left) and GeoB22732 (La Plata Terrace Moat; right) showing polished surfaces and rounded to oblate shapes. (c) Pebbles from Sites GeoB22703 (Ewing Terrace to the north of MdP Canyon; left), GeoB22717 (Ewing Terrace Channel; middle) and GeoB13830 (canyon head; right) showing flatiron shape, faceted faces and striae, which are all typical features of glacially eroded material. See Figures 4a, 5, 6c, and 7a for Parasound profiles across Sites GeoB22732, GeoB22717, GeoB22712, and GeoB22703 respectively.

muscovite-biotite schists. Several small, unidentified lithoclasts exhibited faceted and polished surfaces; one rock fragment with a stoss-and-lee morphology was also identified.

Grab GeoB22716-1, 1,287 water depth. Few medium pebbles (8–16 mm) to cobbles (114 mm) illustrated a lithologic assemblage of medium-grained sandstones, granitoids, and fine-grained, foliated metamorphic rock (one sample). Most of the lithoclasts show faceted surfaces.

Grab GeoB22718-1, 1,411 m water depth. A small amount of granules (2–4 mm) and two cobble sized (101 and 130 mm) rocks were collected and identified as rhyodacite and bioturbated mudstone lithoclast.

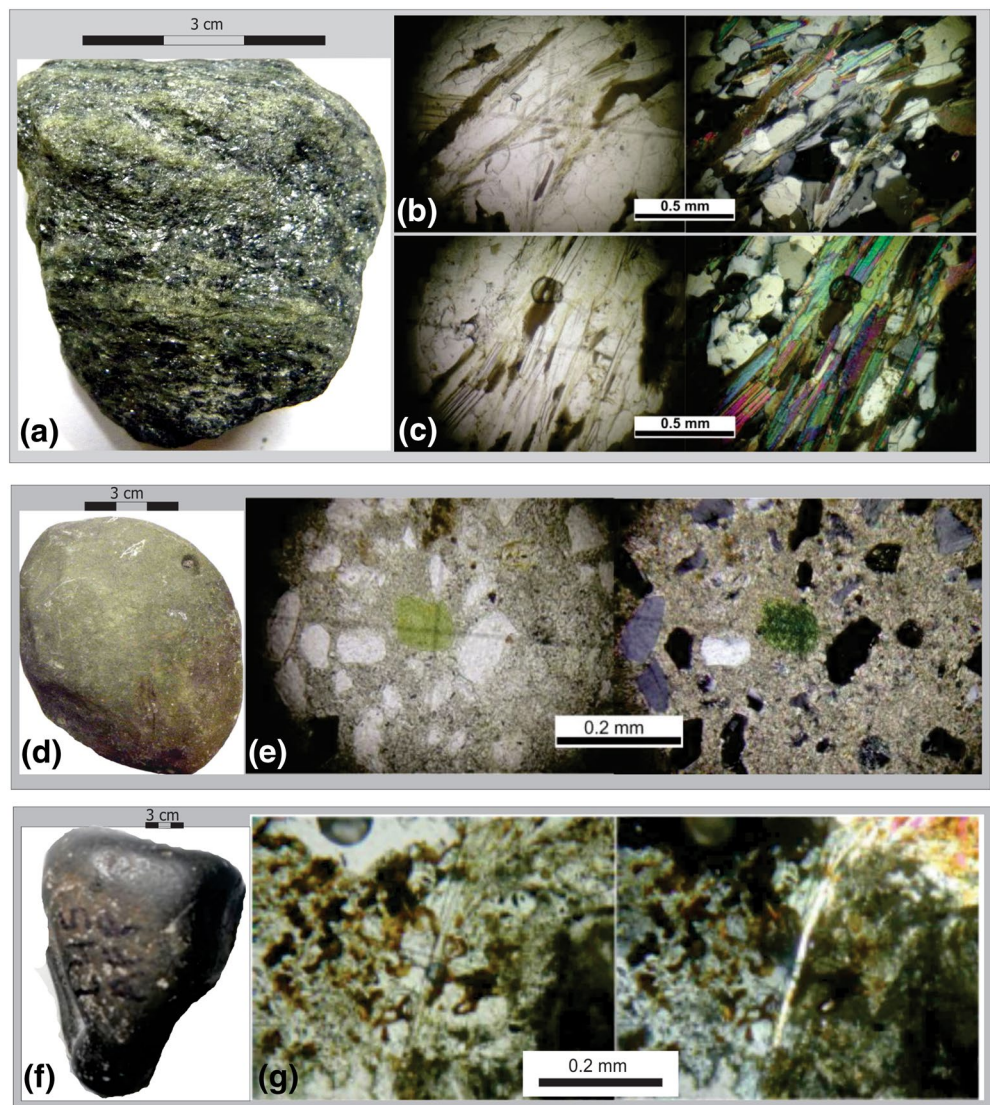


**Figure 9.** The three diagnostic rocks for dropstones source areas. (a) Banded fine-grained schist from Site GeoB22717 (Ewing Terrace Channel). Macroscopic sample; (b) thin section showing a quartz-plagioclase granoblastic aggregate of Q domains interlayered with biotite + sillimanite bundles; (c) this thin section shows a biotite-muscovite interlayering in M domains. See Figure 5 for Parasound profile across Site GeoB22717. (d) Wackestone with micritic cement from Site GeoB22712 (Ewing Terrace Moat). Macroscopic sample; (e) thin section showing the clastic framework dominated by angular to subangular quartz and andesine crystal fragments; rounded volcanic fragments and green glauconite are present in minor proportions. See Figure 6c for Parasound profile across Site GeoB22712. (f) Basalt from Site L45 (lower continental slope north of MdP Canyon). Macroscopic sample; (g) thin section showing dendritic intergrowth of zoisite-opaque minerals and actinolite needles. See Figure 7b for Parasound profile across Site L45.

Gravity core GeoB6816-1, 1,180 m water depth. Few granules (2–4 mm) and a big, black pebble sized rock (50 mm), identified as fine-grained metasediment, were found within a 5-cm thick top layer (Figure 2b) of a gravel rich contourite body (Bozzano et al., 2011).

Gravity core GeoB6813-1, 985 m water depth. Two medium pebbles (10 and 15 mm in size) were found downcore at 62 and 74 cm (Figure 2b), in a gravel-rich, contouritic facies that occupies the upper 74 cm of the core (Bozzano et al., 2011). One specimen was determined as calcareous sandstone with glauconite, glass shards, and pumiceous fragments; the other as volcanoclastic rock (very fine-grained tuff) with incipient internal deformation.

#### 4.2.5. Other Sites from the Continental Slope

Trawling dredge L35, 1,220–1,245 m water depth. The rock assemblage, ranging from medium (8–16 mm) to very coarse pebbles (32–64 mm), was dominated by igneous, both volcanoclastic (very fine-grained tuff) and intrusive (granite or granodiorite), and sedimentary rocks (greenish, very fine-grained sandstones). The surface of the volcanoclastic samples, rough or polished, frequently carried pits and grooves of various shapes (straight, crescentic, irregular) similar to those shown in Figure 8.

Trawling dredge L45, 2,934–2,952 water depth. This is the deepest site, from where several rocks, ranging from medium (8–16 mm) to very coarse pebbles (32–64 mm) in size, were obtained. The assemblage is different from the above described since most rocks display rounded outlines and polished surfaces, often with grooves (straight or concentric), pits and steps. One diagnostic metabasalt exhibited a primary magmatic assemblage represented by relict plagioclase phenocrysts with replacements by hydrated minerals (zoisite in dendritic growth and actinolite) and with vesicles and vugs filled with either opaque minerals, chlorite, zoisite, or zeolite associations (Figures 9f–9g).

Box core GeoB22703-1, 1,320 m water depth. The pebbles from this site, ranging from fine (4–8 mm) to very coarse particles (32–64 mm) in size, were obtained from the sub-seafloor, immersed in a 25 cm-thick, sandy mud interval. The lithology included sandstones, granites, volcanoclastic, metamorphic rocks, and other undefined smaller rock fragments with polished and rounded surfaces. Faceted surfaces were common; stoss-and-lee shape and striae were also observed for two specimens.

Piston core LBIV-5, 616 m water depth. Three rocks, classified as medium-grained sandstone, sienogranite, and metavolcanite, were found at a sediment depth interval between 150 and 156 cm (Figure 2b), where an abrupt boundary between an underlying muddy sediment facies and a topping silty-sandy contouritic facies is developed (Bozzano et al., 2011). The three rocks belong all to the latter silty-sandy facies.

#### 4.3. Water Masses, Current Velocity, and Direction

The vertical water mass distribution in the study area was inferred from vertical potential temperature, salinity and dissolved oxygen profiles obtained by CTD casts at Sites GeoB22718 and GeoB22728 (Figure 2a). The results showed that the middle continental slope is swept by AAIW and UCDW. AAIW is located between 425–450 and 800–1,000 m water depth, underlain by UCDW which occupies the deepest portion of the water column (Figure 10). La Plata Terrace Moat (at 700–800 m water depth) is thus located within AAIW. Ewing Terrace Channel (at 800–1,200 m water depth) and Moat (at 1,100–1,300 m water depth) are mainly controlled by the lower AAIW and by the AAIW-UCDW boundary.

In situ ADCP at Sites GeoB22732 (La Plata Terrace Moat), GeoB22717 (Ewing Terrace Channel), and GeoB22716 (Ewing Terrace Moat) reported data on current velocity and flow direction in the water column down to 70–170 m above seafloor (asf in the following; Figure 10 and Tables S1–S3). Although the reported values do not strictly correspond to the near-bottom current velocity, they reflect the order of magnitude of the regime of the bottom currents that currently operate in the study area. Current velocity at the La Plata Terrace Moat and Ewing Terrace Moat reached  $39 \text{ cm s}^{-1}$  at 70 m asf and  $27 \text{ cm s}^{-1}$  at 170 m asf, respectively, with a flow direction pointing to N-NE. In contrast, current velocity measured in the Ewing Terrace Channel was  $9 \text{ cm s}^{-1}$  at 140 m asf with a flow towards W (Figure 10 and Tables S1–S3).

### 5. Discussion

#### 5.1. Local Versus Remote Provenance of Cobbles and Pebbles

When looking for a source area for these rocks, the Tandilia System could appear as a possibility given its proximity (Figure 1a). This orographic belt reaches the coast at  $38^\circ\text{S}$  and is composed of an igneous metamorphic basement overlain by a sedimentary cover (Cingolani et al., 2011). However, both the sedimentary and volcanic rocks in our collection differ from those of Tandilia. The high content of components of volcanic origin (fragments of volcanic rocks, glass, and pumice) in the sandstones as well as the numerous volcanic rocks, both acidic and basic composition, and tuff, are rare elements in the Tandilia System.

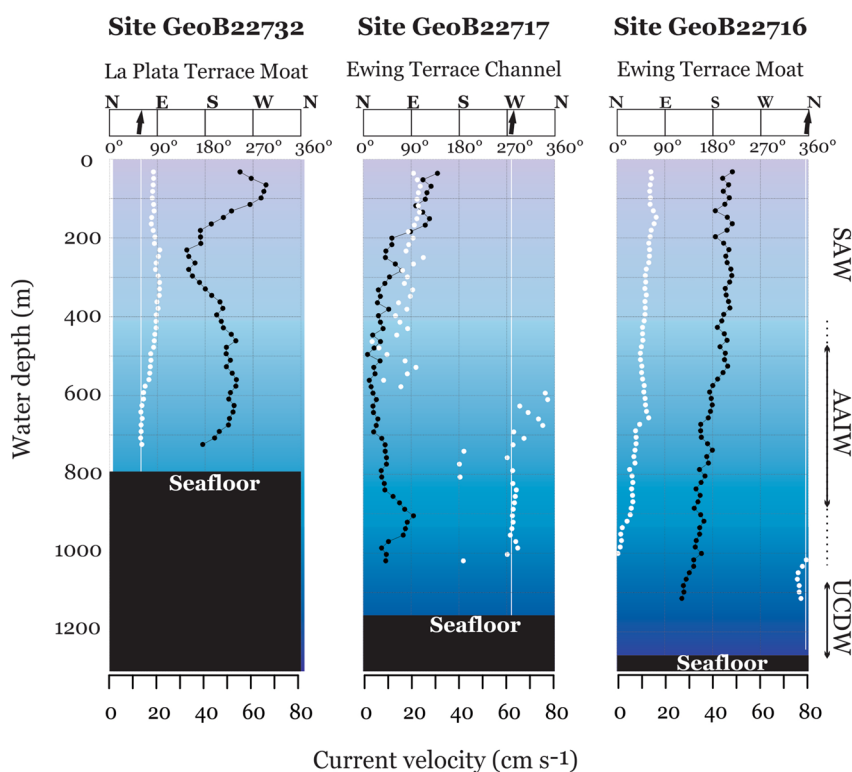


**Figure 10.** Current velocity (black dots) and direction (white dots) measured with ADCP at Sites GeoB22732 (La Plata Terrace Moat), GeoB22717 (Ewing Terrace Channel) and GeoB22716 (Ewing Terrace Moat). Current directions: 0° = North; 90° = East; 180° = South and 270° = West. Vertical white line marks current direction close to the bottom. Water mass vertical distribution obtained from CDT casting at Sites GeoB22718 and GeoB22728. AAIW, Antarctic Intermediate Water; SAW, Sub-Antarctic Water; UCDW, Upper Circumpolar Deep Water.

Most of our rock specimens show numerous features of surface morphology that point to glacial erosion. Namely, the two plausible source areas for glaciogenic material in the study area are Patagonia and Antarctica. Patagonia underwent several glaciations during Neogene and Quaternary times (Mercer, 1976). During the Great Patagonia Glaciation (GPG, 1.168 and 1.016 Ma), glacier tongues reached the Atlantic coast (Rabassa & Clapperton, 1990; Rabassa et al., 2005) and expanded onto the continental shelf only off the Strait of Magellan and south of the Rio Gallegos Valley (52°30'S; Caldenius, 1932). Submerged moraines related to the GPG have been found off northern Tierra del Fuego at 60 m modern water depth, 45 km offshore of the present coastline (Isla & Schnack, 1995). During the last glacial period, the Patagonian Ice Sheet (PIS) extended along the crest of the Andean Cordillera, between latitudes 38°S and 55°S, as a continuous, narrow and elongated icecap (Davies et al., 2020; Figure 1a). In the northern sector of PIS, glacial outwash plains drained westward while the ice field expansion to the eastern side of the Andes was limited and did not exceed longitude 71°W (Glasser et al., 2008; Hulton et al., 2002). At those times, the Patagonian rivers made a significant contribution of material to the coast by accumulating gravel and sand beds (called “Rodados Patagónicos”), which are distributed from the north flank of the Colorado River (40°S) to Tierra del Fuego (55°S) (Figure 1a). They consist of rounded gravel clasts in a finer matrix, with pebbles and cobbles of highly variable lithology. The genesis of this coarse material is attributed to glaciofluvial processes in southern Patagonia and to fluvial and piedmont processes in northern Patagonia (Martínez et al., 2009). Although this coarse material could have been incorporated into the ocean realm by gravity-induced down-slope processes at times of low sea level, subsequent northward transport to the latitudes of the study area by bottom currents seems unlikely. Only small-sized rocks from nearby local sources may have been transported by rivers and transferred to the MdP area by along-slope processes (Bozzano et al., 2011).

Multiple transfer mechanisms can deliver fine-grained glacially eroded sediments deep into the ocean but only ice-rafting can provide coarse-grained cobble-sized material (Cook et al., 2017). We would exclude the

contribution of rocks from continental glaciers lobes and associated outwash plains, drained by glaciofluvial transport to the study area. Thus, we interpret most of the rocks, found in the MdP Canyon area, as IRD due to the wide range in lithology, wide grain-size spectrum decoupled from the hosting background sediment, the glacial morphology imprinted on the rocks surface, and the presence of cobbles far from the shelf break (Bennett et al., 1996; Conolly & Ewing, 1965; Wentworth, 1936).

Glaciations on the Antarctic continent started with the opening of the Drake Passage and the associated new circumpolar circulation approximately at the Eocene-Oligocene boundary, that is, 34 Ma years ago (Bell & Seroussi, 2020, and references therein). Through the late Pleistocene, the ice in East and West Antarctica expanded and reached the edge of the continental shelf during cool periods and retreated during warm periods (Bell & Seroussi, 2020). The recurrent growth and decline of ice sheets, especially in West Antarctica, generated large amounts of IRD to be distributed across the South Atlantic.

These IRD distribution patterns have been recently investigated since they provide valuable information on the past variability of the Antarctic ice shield (Weber et al., 2018). IRD deposits have been frequently reported for both glacial and interglacial periods off Antarctica, in the Scotia Sea and across the southernmost South Atlantic (Ciesielski et al., 1982; Conolly & Ewing, 1965; Diekmann et al., 2000, 2003; Hodell et al., 2001; Noble et al., 2012; Teitler et al., 2010; Weber et al., 2014). Diekmann et al. (2003) have observed major supply of terrigenous sediments to the temperate regions of the South Atlantic during glacial periods, whereas, in the polar region, IRD fluxes would increase at the glacial terminations, with short-term peaks also in MIS 2 and MIS 3. This is in line with other authors that have pointed out that IRD may have traveled over long distances during glacial periods, whereas the material has dropped in close proximity to its southern origin during interglacials (Keany et al., 1976; Watkins et al., 1974).

The northernmost locations, where IRD has previously been reported off the Argentine margin so far, corresponds to the Patagonian lower continental slope at roughly 47°S (Ivanova et al., 2018) and the Maurice Ewing Bank, east of the Falkland (Malvinas) Islands (50°S; Ciesielski et al., 1982). There, the highest proportions of IRD date back to 1–0.7 Ma with a positive temporal correlation between IRD abundance and GPG extent. According to Plafker et al. (1977) and Bornhold (1983), both Antarctica and Tierra del Fuego could have provided dropstones to Falkland (Malvinas) Plateau and Maurice Ewing Bank. No other studies have later attempted to address the challenge of spotting the source areas for coarse-sized IRD found in the South Atlantic realm. In fact, geological surveys in these remote and vast areas, which are covered by continental ice most of the year, are limited and patchy. This restriction makes it difficult to find the exact correspondence between the petrography of dropstones and a specific regional rocky outcrop (Licht & Hemming, 2017). Based on three diagnostic types of rocks, we suggest Antarctic Peninsula, the sub-Antarctic islands, and Tierra del Fuego as probable source regions for the IRD found around the MdP Canyon.

## 5.2. Morpho-Petrography and Provenance of the Ice-Rafted Debris

The first diagnostic rock type, recovered at Site L45, has a basic metavolcanic composition showing large replacement patches of zoisite, actinolite, opaque minerals, and quartz (Figures 9f–9g). This mineral assemblage resembles the Mesozoic mafic igneous rocks commonly reported as the Rocas Verdes (“green rocks”) ophiolite complexes (Dalziel et al., 1974; Stern & De Wit, 2003). These rocks have been interpreted as remnants of progressive stages in the development of oceanic-type crust in a tectonic back-arc basin situation. This configuration had evolved along mid-ocean-ridge-type spreading centers during the initial stage of the Gondwana breakup (Stern & De Wit, 2003). Ophiolitic remnants of the Rocas Verdes marginal basin crop out nowadays along a discontinuous belt in the Patagonian and Fuegian Andes between 51° and 56°S (Figure 1a). They also occur on the island of South Georgia, Scotia Sea (Larsen Harbour complex) and on the southwestern Navarino Island, Tierra del Fuego, Patagonia (Tortuga complex; Calderón et al., 2016; Mukasa & Dalziel, 1996; Stern & De Wit, 2003).

The second diagnostic rock type, collected at Sites GeoB22717 and GeoB22712, consists of a few specimens of fine-grained muscovite-biotite schists of high to medium grade metamorphism (Figures 9a–9c). They may belong to the Cordillera Darwin Metamorphic Complex (Tierra del Fuego, see Figure 1a) whose deformation and high-grade metamorphism has been associated with the closure of the Rocas Verdes Basin (Dalziel et al., 1974). In this complex, rocks of a high metamorphic grade, containing staurolite and sillimanite, have

been described (Hervé et al., 2010). An isolated mention of high-grade metamorphic rocks with sillimanite has also been reported from Cape Dubouzet, northern Antarctic Peninsula (Hervé et al., 1996).

The third diagnostic rock type is represented by the large population of yellowish micritic wackestones (recovered at Sites GeoB13830 and GeoB22712), composed of angular quartz and feldspar grains, abundant lithic fragments of volcanic origin, pumice, glass shards, and glauconite (Figures 9d and 9e). This heterogeneous assemblage indicates an active volcanic source area nearby during original sedimentation of these rocks as well as a shelf environment for an initial deposition (glauconite as indicator). The Cretaceous marine deposits in the James Ross Island basin, located at the northeastern tip of the Antarctic Peninsula, seem to be a plausible source area for these rocks. Here, marine strata deposited within a retro-arc basin with sediment supply from an active magmatic arc (now represented by the Antarctic Peninsula) are nowadays exposed in 1,500–2,000-m thick outcrops (Crame et al., 1991). The entire sequence is divided into the Gustav and Marambio Groups (Crame et al., 1991; Ineson et al., 1986; Rinaldi et al., 1978). Within the Marambio Group, the López de Bertodano Formation displays mudstones and silty sandstones, with a minor contribution of calcareous facies attributed to a shallow-marine paleo-environment. Volcanoclastic lithologies, tuff, and glauconite have been observed in the upper part of this formation (Crame et al., 1991).

### 5.3. Icebergs Trajectory and Ice-Rafted Debris Transport

In the present day, large icebergs usually tend to stay close to the coast, drift under the Coriolis-related forcing around Antarctica embedded in the Antarctic Coastal Current in a counter-clockwise direction and accumulate in the Weddell Sea (Figure 1b; Gladstone et al., 2001; Rackow et al., 2017; Stuart & Long, 2011; Tournadre et al., 2012, 2016). Here, icebergs may follow two distinct directions: those located west of 40°W are exported into the Scotia Sea between Elephant and South Orkney Islands; those located east of 40°W follow the eastward course of the Weddell Gyre (Schodlok et al., 2006) and enter the ACC to the east. A small amount of icebergs leave the coastal current under the effect of katabatic winds in three specific sectors: the Weddell Sea, near the Kerguelen Plateau and the Ross Sea. Once in the open ocean, they drift following the clockwise flow of the ACC (Rackow et al., 2017; Stuart & Long, 2011; Tournadre et al., 2016). Subsequent iceberg motion is broadly similar in direction to that of the wind and currents (Gladstone et al., 2001); thus, icebergs calving from the Western Antarctic Peninsula and West Antarctica ice sheets have the best options to reach the northern latitudes of the Antarctic Pacific Sector, enter the Scotia Sea and continue north to the southern margin of Argentina (Brown et al., 2017; López-Martínez et al., 2011).

According to morphological analyses of plough marks, carved into Patagonian shelf and upper slope sediment (at 73–685 m modern water depths), large icebergs, up to 500 m thick and 2 km wide, have frequently drifted along the Argentine Margin during glacial times (López-Martínez et al., 2011). Plow marks observed in the North Falkland (Malvinas) Basin further corroborate that these icebergs, scouring the seafloor at present-day water depths from 280 to 460 m, were carried by the eastern branch of the FMC, circumventing the islands from the east (Brown et al., 2017). Once along the Argentine margin, icebergs would follow quasi-linear trajectories to the north. In fact, it has been observed that drifter trajectories extend from the Drake Passage to the Brazil-Falkland (Malvinas) Confluence Zone in smooth tracks, without describing convoluted loops that usually characterize the path of unstable ocean currents (Figures 1a; Artana et al., 2016, 2018; Matano et al., 2010). Satellite images have shown floating iceberg fleets cross the Drake Passage after having left the West Antarctic coast, turn into northwestern direction, drift around the Falkland (Malvinas) Islands, and proceed finally towards the north. During their journey to the north, modern icebergs experience a significant reduction in size by melting and fracturing. Only a few small remains of the original iceberg will eventually end up in the study area.

From what was known so far, it was, thus, not expected that IRD may have been supplied in large quantities to the study area in the past. However, glacial scenarios may differ from current ones. Rapid ice stream destabilization events during major deglaciation or ice sheet collapse might have produced larger volumes of icebergs (>500 m thick), and carried larger amounts of detritus than seen in today's icebergs (Williams et al., 2010). Also in the Western North Atlantic, icebergs traveled a thousand kilometers away from the polar regions and reached low latitudes (~33°N) during glacial and post-glacial periods (Hill et al., 2008). During the Last Glacial Maximum (LGM; 26.5–19 cal ka BP; Clark et al., 2009), sea-surface temperatures in

the South Atlantic were approximately 4°C degrees lower than today (Annan & Hargreaves, 2013; Gersonde et al., 2005). West and East Antarctic Ice Sheets (WAIS and EAIS) as well as the Antarctic Peninsula Ice Sheet (APIS) expanded onto the outer continental shelf or up to the shelf break (e.g., Bentley et al., 2014; Cofaigh et al., 2014; Mackintosh et al., 2014). The Winter Sea Ice (WSI) extended at least 5° further north than it does today, reaching the Falkland (Malvinas) Trough (52°S) until 19 cal ka BP while the Summer Sea Ice (SSI) extended to 59°S between 30 and 22 ka (Allen et al., 2011). The expansion of both SSI and WSI fields, even during a pre-LGM time, has been further confirmed by other studies (Collins et al., 2012). As for the sub-Antarctic islands, the South Orkney and South Shetlands islands show evidences of LGM ice expansion on their shelves, whereas in South Georgia Island one or more glaciations have extended to the continental shelf break earlier than LGM (Hodgson et al., 2014). Retreat from LGM was not synchronous around the Antarctic margin (Bentley et al., 2014). It initiated on the outer shelf of the northern Antarctic Peninsula between 19 and 18 cal ka BP (Heroy & Anderson, 2007; Mackintosh et al., 2014; Weber et al., 2014), although the majority of Antarctic ice sheets retreated between 15 and 12 cal ka BP, with a peak in ice-sheet collapse around 14 cal ka BP coinciding with Meltwater Pulse 1a (Fogwill et al., 2017). The ice sheets continued to decay into the Holocene before reaching the present-day configuration between 7 and 6 cal ka BP (Anderson et al., 2002; Mackintosh et al., 2011, 2014; Weber et al., 2014).

It is not an easy task to establish the timing of IRD deposition in the MdP Canyon area because the rock specimens rest, in most cases, on the modern seafloor as loose, that is, not buried, deposits. Since the depositional age of the rocks themselves cannot be determined, dating basically relies on the surrounding and covering sediment. One isolated pebble was found at 100 cm sediment depth in Core T300 and a CWC fragment, which was found 16 cm above this pebble, has been dated to  $15.5 \pm 0.25$  cal ka BP (Figure 2b). Assuming a constant average sedimentation rate at this site ( $5.3\text{--}5.5$  cm  $\text{ka}^{-1}$ ) over time, we can estimate an age of about 18.9–18.2 cal ka BP for the deposition of the pebble. This estimate would allow to link the episode of its drifting toward the MdP Canyon area with the early stages of the Antarctic Peninsula Ice Sheet retreat which has started between 19 and 18 cal ka BP (Heroy & Anderson, 2007; Mackintosh et al., 2014; Weber et al., 2014). The sedimentary infills of plough marks along the Patagonian margin and in the north Falkland (Malvinas) Basin have also been attributed to the LGM to early deglaciation time interval (Brown et al., 2017; López-Martínez et al., 2011). These landforms, showing good preservation and only a thin sediment cover, reach maximum modern water depths of 685 m at the Patagonia slope and 460 m in the northern Falkland (Malvinas) Basin. These deep-water locations, unusual for plough marks, provide evidence for the outstanding size of the icebergs and their bottom-scouring keels (500 m), in combination with a glacial sea level, which was about 105 m lower than today (Guilderson et al., 2000). Although the global average values for LGM lowstand are  $-125$  m (e.g., Hanebuth et al., 2000), the Argentinean sea level curve needs to be adjusted to 105 m for additional glacio-isostatic and tectonic uplift components (Guilderson et al., 2000).

#### 5.4. Bottom Currents and Ice-Rafted Debris Distribution

The lithic IRD material, initially incorporated inside the icebergs or draping their surfaces, deposits with ice melting, sinks down during drifting as isolated dropstones or in the form of sediment clouds, or dumps as mass when an iceberg ultimately stops traveling (Gilbert, 1990). Abundant IRD in the MdP Canyon area has probably resulted from large iceberg fleets being blocked by and melting at the Brazil-Falkland (Malvinas) Confluence Zone, since this area is characterized by a steep temperature gradient (Gordon, 1989).

Those dropstones that were found randomly scattered over a wide geographic area along the middle slope were loosely added to the hemipelagic/contouritic seabed sediment. After deposition, two possible mechanisms might have secondarily modified their distribution. As a first likely scenario, the intense slope-parallel contour currents, which led to effective erosion over geological times and formed abundant furrows, scours and moats, have gradually winnowed the finer sediment fractions out of the coarse sediment, leaving the larger dropstones as a lag deposit at their original emplacement. This mechanism would, however, only explain the presence of dropstones within erosional, contouritic features.

IRD was also found inside the canyon head (Sites GeoB13830, T300), on a small terrace at the middle slope (Site GeoB22703), and at the foot of the canyon wall at the lower slope (Site L45), where the action of contouritic bottom currents has to be expected of being less intense. In addition, dropstones were recovered



from the downslope directed Ewing Terrace Channel (Site GeoB22717), where no along-slope, current-driven processes are expected to act and where the modern current velocity was as low as  $9 \text{ cm s}^{-1}$  at 140 m asf (Figure 10 and Table S2). Thus, along-slope transport processes alone cannot explain the IRD concentration inside the bathymetric depressions in the MdP canyon area.

As an alternative scenario, dropstones were originally scattered over wide parts of the continental slope, including the edges of morphological depressions (channels, moats, canyon heads, and sidewalls). The rocks eventually fell into these depressions mainly driven by gravity as mass-wasting deposits. This process might have been supported by the erosional effect of the bottom currents in some cases, and by slumping, slope failure, and other gravity-induced events, which commonly occur in blind, slope-confined canyons (Farre et al., 1983; Harris & Whiteway, 2011). The latter case would apply to the canyon head area, downslope Ewing Terrace Channel, and the northern wall of the canyon (Site L45). Here, IRD accumulation has probably resulted solely from instability of the channel/canyon walls, as no along-slope processes can be advocated that were able to remove the fines. In the canyon head area (Core GeoB13830-1), dropstones were, in fact, found 4–22 cm below the modern sediment surface and dropstones were also immersed in fine, silty sediment at Site GeoB22717 (Ewing Terrace Channel). Where, in contrast, efficient bottom currents were at place, mass-wasting deposits would experience reworking by bottom currents, which finally removed the fines and erased any evidence of gravity-induced process. These mixed downslope and along-slope processes could explain the dropstone accumulation in the Ewing Terrace Moat and in the La Plata Terrace Moat. Both erosional features show distinct asymmetric sidewalls with a staircase-like morphology at the western side (i.e., landward/upslope) and local contourite drift bodies covering the eastern side (i.e., seaward/downslope; Figures 4 and 6). This particular geometry suggests that the bottom currents are routed by Coriolis-induced helical flows, which favor the entrenchment of the thalweg into the pre-existing, flat-lying hardrock slope substrate with a progressively upslope migrating dynamic (Steinmann et al., 2020). This migration could lead to local erosion of sediment at the western slope, which, in turn, would continuously enrich dropstones, stemming from the eroded material, at the moat floor. Afterward deposition in these conduit elements, the local bottom currents would concentrate these dropstone layers by further eroding the moat thalwegs. The measured modern bottom current velocity is high enough ( $30\text{--}40 \text{ cm s}^{-1}$ ) to mobilize grain sizes up to medium sand (McCave, 2008), leaving the coarsest fraction (coarse sand to pebbles) as loose lag layer. Recent studies have reported current velocities up to  $52 \text{ cm s}^{-1}$  within the Ewing Terrace Moat associated with turbulence induced by irregular and steep topography (Steinmann et al., 2020). Past oceanographic bottom regime in the Ewing Terrace and La Plata Terrace moats probably achieved similar range of magnitude than today, as it is reflected by the long-lasting presence of these erosional elements. This interpretation is in line with other studies from the NE Atlantic region, where dropstones have been found up-concentrated in scour pits and erosional furrows as the result of bottom winnowing processes (Lim et al., 2017; Masson et al., 2004). Large IRD accumulations have also been interpreted as residual lag after intense bottom current circulation at the Maurice Ewing Bank, SW Atlantic (Ciesielski et al., 1982).

## 6. Conclusions and Wider Implications

This is the first discovery of large quantities of coarse-grained material (gravel, pebble, and cobble) which has rafted from the southern polar regions as far north as to the MdP Canyon area ( $38^\circ\text{S}$ , Western South Atlantic). Detailed petrographic and morphological analyses allowed for defining these rock specimens as IRD.

The Antarctic Peninsula, sub-Antarctic islands in the Scotia Sea, and Tierra del Fuego are plausible source areas for the discovered ice-rafted material depositing at lower latitudes along the Argentine margin. The depositional age of one dropstone, estimated to about 18.9–18.2 cal ka BP, suggests that the rafting process to the MdP Canyon area took place at an early stage of post-LGM deglaciation and in association with an initial instability of the Antarctic Peninsula Ice Sheet.

Large icebergs, first trapped in the Antarctic Circumpolar Circulation, rafted coarse detritus over thousands of kilometers to the north, from Antarctica along the trajectory of the Falkland (Malvinas) Current following the ACM. This finding requires that the icebergs had enormous sizes since they survived long enough to reach lower latitudes until they arrived at the barrier of the Brazil-Falkland (Malvinas) Confluence Zone.

This focused dropstone deposition in the MdP Canyon area (38°S) resulted from mayor ice melting exactly at this latitude because here the cold Falkland (Malvinas) Current encountered the warm BC. Gravity-induced and bottom-current related erosional but also sedimentary processes explain why IRD accumulation showed its highest concentrations within morphological depressions in the study area.

Our findings confirm previous evidence, deduced from plough marks at the seafloor of the Patagonian margin and North Falkland (Malvinas) Basin, indicating the existence of very large icebergs at the end of the LGM and during the following deglaciation that drifted with the Falkland (Malvinas) Current along the Argentine margin. This fact bears some wider implications: glacial sea-ice might have extended far beyond the northernmost limit reached by ice in winter today; ice sheet instability seems to have started as early as at the beginning of deglaciation with iceberg fleets released into the Southern Atlantic; and lower to mid-latitudes sea-surface temperatures might have been substantially colder at that time than today, allowing the icebergs to melt relatively late during their northward journey.

As for the dropstone blankets, they seem to provide the hard substrate needed by benthic megafauna and CWCs to colonize the seafloor under a deep-water, high-speed bottom-current regime (Ziegler et al., 2017). This connection is of particular interest in the MdP area where a giant CWC mound province has been recently discovered (Steinmann et al., 2020). Thus, the understanding of the (paleo)oceanographic and sedimentary factors that have regulated the dropstone distribution on the ocean margin are of broad and interdisciplinary relevance for studies related to the heterogeneity of marine habitats.

## Data Availability Statement

The multibeam EM122 data, transit of SONNE cruise SO260/1 (South Atlantic), will be available by accessing PANGAEA Data Publisher for Earth & Environmental Science at <https://www.pangaea.de> with DOI 10.1594/PANGAEA.888569.

## References

- Allen, C. S., Pike, J., & Pudsey, C. J. (2011). Last glacial–interglacial sea-ice cover in the SW Atlantic and its potential role in global deglaciation. *Quaternary Science Reviews*, 30, 2446–2458.
- Anderson, J. B., Shipp, S. S., Lowe, A. L., Wellner, J. S., & Mosola, A. B. (2002). The Antarctic Ice Sheet during the Last Glacial Maximum and its subsequent retreat history: A review. *Quaternary Science Reviews*, 21(1–3), 49–70.
- Annan, J. D., & Hargreaves, J. C. (2013). A new global reconstruction of temperature changes at the Last Glacial Maximum. *Climate of the Past*, 9, 367–376.
- Artana, C., Ferrari, R., Koenig, Z., Saraceno, M., Piola, A. R., & Provost, C. (2016). Malvinas Current variability from Argo floats and satellite altimetry. *Journal of Geophysical Research: Oceans*, 121(7), 4854–4872. <https://doi.org/10.1002/2016JC011889>
- Artana, C., Lellouche, J.-M., Sennéchal, N., & Provost, C. (2018). The open-ocean side of the Malvinas Current in Argo floats and 24 years of Mercator Ocean high-resolution (1/12) physical reanalysis. *Journal of Geophysical Research: Oceans*, 123, 8489–8507. <https://doi.org/10.1029/2018JC013887>
- Bell, R. B., & Seroussi, H. (2020). History, mass loss, structure, and dynamic behavior of the Antarctic Ice Sheet. *Science*, 20, 1321–1325.
- Bennett, M. R., Doyle, P., & Mather, A. E. (1996). Dropstones: Their origin and significance. *Palaeogeography, Palaeoclimatology, Palaeoecology*, 121, 331–339.
- Bentley, M. J., Cofaigh, C. O., Anderson, J. B., Conway, H., Davies, B., Graham, A. G., et al. (2014). A community-based geological reconstruction of Antarctic Ice Sheet deglaciation since the Last Glacial Maximum. *Quaternary Science Reviews*, 100, 1–9.
- Bornhold, B. D. (1983). Ice-rafted debris in sediments from Leg 71, Southwest Atlantic Ocean. In W. J. Ludwig, V. A. Krasheninnikov, S. W. Wise, Jr. (Eds.), *Initial reports of the deep sea drilling program* (Vol. 71). Washington, DC: Washington U.S. Government Printing Office. <https://doi.org/10.2973/dsdp.proc.71.110.1983>
- Bozzano, G., Martín, J., Spoltore, D. V., & Violante, R. A. (2017). Los cañones submarinos del Margen Continental Argentino: Una síntesis sobre su génesis y dinámica sedimentaria. *Latin American Journal of Sedimentology and Basin Analysis*, 24(1), 85–101.
- Bozzano, G., Violante, R. A., & Cerredo, M. E. (2011). Middle slope contourite deposits and associated sedimentary facies off NE Argentina. *Geo-Marine Letters*, 31(5–6), 495–507.
- Brown, C. S., Newton, A. M. W., Huuse, M., & Buckley, F. (2017). Iceberg scours, pits, and pockmarks in the North Falkland Basin. *Marine Geology*, 386, 140–152.
- Caldenius, C. C. Z. (1932). Las Glaciaciones Cuaternarias en la Patagonia y Tierra del Fuego: Una investigación regional, estratigráfica y geocronológica—Una comparación con la escala geocronológica sueca. *Geografiska Annaler*, 14(1–2), 1–164.
- Calderón, M., Hervé, F., Fuentes, F., Fossdick, J. C., Sepúlveda, F., & Galaz, G. (2016). Tectonic evolution of Paleozoic and Mesozoic Andean metamorphic complexes and the Rocas Verdes Ophiolites in southern Patagonia. In M. C. Gigliome (Ed.), *Geodynamic evolution of the Southernmost Andes* (pp. 7–36). Cham, Switzerland: Springer Earth System Sciences. [https://doi.org/10.1007/978-3-319-39727-6\\_2](https://doi.org/10.1007/978-3-319-39727-6_2)
- Ciesielski, P. R., Ledbetter, M. T., & Ellwood, B. B. (1982). The development of Antarctic glaciation and the Neogene paleoenvironment of the Maurice Ewing Bank. *Marine Geology*, 46, 1–5.

## Acknowledgments

Ines Voigt commenced this study while performing her Ph.D. at MARUM (Bremen). Daniel Lauretta (Argentine Museum of Natural Sciences, Buenos Aires) provided the lithic fraction from the trawling dredges L35 and L45. The sediment core descriptions of Conrad Core RC12-249 and Vema Core VM12-27 were performed by A. Raring and E. Dabberg, respectively. The authors are grateful to the captains, crew and participants of research cruises M78/3a and SO260/1. Very special thanks go to the scientific members of both geology teams. Adriana Blasi, Daniel Poiré and Alejandro Ribot (National University of La Plata), José Luis Panza and Julio Cobos (SEGEMAR, Buenos Aires) as well as Juan Manuel Lirio and Rodolfo Del Valle (Argentine Antarctic Institute, Buenos Aires) are acknowledged for an initial discussion of the rock petrography and the associated source areas. The authors thank the journal's editor, Peter van der Beek, Michael Weber, and an anonymous reviewer for their thoughtful comments, which greatly helped to improve the quality of the work. RV Sonne Expedition SO260 was funded by and carried out in the framework of the DFG Research Centre/Cluster of Excellence “The Ocean in the Earth System” (MARUM – Center for Marine Environmental Sciences at the University of Bremen). Cruise SO260 received additional funding from the Helmholtz Association (Alfred Wegener Institute Helmholtz Centre for Polar and Marine Research, Bremerhaven).

- Cingolani, C. A. (2011). The Tandilia System of Argentina as a southern extension of the Río de la Plata craton: An overview. *International Journal of Earth Sciences*, *100*(2–3), 221–242.
- Clark, P. U., Dyke, A. S., Shakun, J. D., Carlson, A. E., Clark, J., Wohlfarth, B., et al. (2009). The Last Glacial Maximum. *Science*, *325*, 710–714.
- Cofaigh, C. Ó., Davies, B. J., Livingstone, S. J., Smith, J. A., Johnson, J. S., Hocking, E. P., et al. (2014). Reconstruction of ice-sheet changes in the Antarctic Peninsula since the Last Glacial Maximum. *Quaternary Science Reviews*, *100*, 87–110.
- Collins, L. G., Pike, J., Allen, C. S., & Hodgson, D. A. (2012). High-resolution reconstruction of southwest Atlantic sea-ice and its role in the carbon cycle during marine isotope stages 3 and 2. *Paleoceanography*, *27*(3), 27. <https://doi.org/10.1029/2011PA002264>
- Conolly, J. R., & Ewing, M. (1965). Ice-Rafted Detritus as a climatic indicator in Antarctic deep-sea cores. *Science*, *150*, 1822–1824.
- Cook, C. P., Hemming, S. R., van de Flierdt, T., Davis, E. L., Williams, T., Galindo, A. L., et al. (2017). Glacial erosion of East Antarctica in the Pliocene: A comparative study of multiple marine sediment provenance tracers. *Chemical Geology*, *466*, 199–218.
- Crame, J. A., Pirrie, D., Riding, J. B., & Thomson, M. R. A. (1991). Campanian–Maastrichtian (Cretaceous) stratigraphy of the James Ross Island area, Antarctica. *Journal of the Geological Society*, *148*(6), 1125–1140.
- Dalziel, I. W. D., de Wit, M. F., & Palmer, K. F. (1974). Fossil marginal basin in the southern Andes. *Nature*, *250*, 291–294.
- Davies, B. J., Darvill, C. M., Lovell, H., Bendle, J. M., Dowdeswell, J. A., Fabel, D., et al. (2020). The evolution of the Patagonian Ice Sheet from 35 ka to the present day (PATICE). *Earth-Science Reviews*, *204*, 103152.
- Diekmann, B., Fütterer, D. K., Grobe, H., Hillenbrand, C. D., Kuhn, G., Michels, K., et al. (2003). Terrigenous sediment supply in the polar to temperate South Atlantic: Land-ocean links of environmental changes during the late quaternary. In G. Wefer, S. Mulitza, & V. Ratmeyer (Eds.), *The South Atlantic in the late quaternary: Reconstruction of material budgets and current systems* (pp. 375–399). Berlin, Heidelberg: Springer-Verlag.
- Diekmann, B., Kuhn, G., Rachold, V., Abelman, A., Brathauer, U., Fütterer, D. K., et al. (2000). Terrigenous sediment supply in the Scotia Sea (Southern Ocean): Response to Late Quaternary ice dynamics in Patagonia and on the Antarctic Peninsula. *Palaeogeography, Palaeoclimatology, Palaeoecology*, *162*(3–4), 357–387.
- Farre, J. A., McGregor, B. A., Ryan, W. B., & Robb, J. M. (1983). *Breaching the shelfbreak: Passage from youthful to mature phase in submarine canyon evolution* (Vol. 33, pp. 2539). Broken Arrow, OK: The Society of Economic Paleontologists and Mineralogists Special Publication.
- Fogwill, C. J., Turney, C. S. M., Gollledge, N. R., Etheridge, D. M., Rubino, M., Thornton, D. P., et al. (2017). Antarctic ice sheet discharge driven by atmosphere-ocean feedbacks at the Last Glacial Termination. *Scientific Reports*, *7*(1), 1–10. <https://doi.org/10.1038/srep39979>
- Frank, N., Paterne, M., Ayliffe, L. K., van Weering, T., Henriot, J.-P., & Blamart, D. (2004). Eastern North Atlantic deep-sea corals: Tracing upper intermediate water D14C during the Holocene. *Earth and Planetary Science Letters*, *219*(3–4), 297–309.
- Garcia, C. A., Sarma, Y. V., Mata, M. M., & Garcia, V. M. (2004). Chlorophyll variability and eddies in the Brazil–Malvinas Confluence region. *Deep Sea Research Part II: Topical Studies in Oceanography*, *51*(1–3), 159–172.
- Gersonde, R., Crosta, X., Abelman, A., & Armand, L. (2005). Sea-surface temperature and sea ice distribution of the Southern Ocean at the EPILOG last glacial maximum—A circum-Antarctic view based on siliceous microfossil records. *Quaternary Science Reviews*, *24*(7–9), 869–896.
- Gilbert, R. (1990). Rafting in glacial marine environments. *Geological Society, London, Special Publications*, *53*(1), 105–120.
- Gladstone, R. M., Bigg, G. R., & Nicholls, K. W. (2001). Iceberg trajectory modeling and meltwater injection in the Southern Ocean. *Journal of Geophysical Research*, *106*(C9), 19903–19915. <https://doi.org/10.1029/2000JC000347>
- Glasser, N. F., Jansson, K. N., Harrison, S., & Kleman, J. (2008). The glacial geomorphology and Pleistocene history of South America between 38 S and 56 S. *Quaternary Science Reviews*, *27*(3–4), 365–390.
- Goodell, H. G. (1964). Marine geology of the Drake Passage Scotia Sea, and South Sandwich Trench. In: *USNS ELTANIN marine geology cruises 1-8. Sedimentology research laboratory contribution N* (Vol. 7, p. 263). Tallahassee, FL: Department of Geology, Florida State University.
- Gordon, A. L. (1989). Brazil-Malvinas Confluence – 1984. *Deep-Sea Research Part A Oceanographic Research Papers*, *36*(3), 359–384.
- Guilderson, T. P., Burckle, L., Hemming, S., & Peltier, W. R. (2000). Late Pleistocene sea level variations derived from the Argentine Shelf. *Geochemistry, Geophysics, Geosystems*, *1*(12), 2000GC000098. <https://doi.org/10.1029/2000GC000098>
- Hanebuth, T., Statteger, K., & Grootes, P. M. (2000). Rapid flooding of the Sunda Shelf: A late-glacial sea-level record. *Science*, *288*(5468), 1033–1035.
- Harris, P. T., & Whiteway, T. (2011). Global distribution of large submarine canyons: Geomorphic differences between active and passive continental margins. *Marine Geology*, *285*(1–4), 69–86.
- Hernández-Molina, F. J., Paterlini, M., Violante, R., Marshall, P., de Isasi, M., Somoza, L., & Rebesco, M. (2009). Contourite depositional system on the Argentine Slope: An exceptional record of the influence of Antarctic water masses. *Geology*, *37*(6), 507–510.
- Heroy, D. C., & Anderson, J. B. (2007). Radiocarbon constraints on Antarctic Peninsula Ice Sheet retreat following the Last Glacial Maximum (LGM). *Quaternary Science Reviews*, *26*, 3286–3297.
- Hervé, F., Fanning, C. M., Pankhurst, R. J., Mpodozis, C., Klepeis, K., Calderón, M., & Thomson, S. N. (2010). Detrital zircon SHRIMP U–Pb age study of the Cordillera Darwin Metamorphic Complex of Tierra del Fuego: Sedimentary sources and implications for the evolution of the Pacific margin of Gondwana. *Journal of the Geological Society*, *167*(3), 555–568.
- Hervé, F., Lobato, J., Ugalde, I., & Pankhurst, R. J. (1996). The geology of Cape Dubouzet, northern Antarctic Peninsula: Continental basement to the Trinity Peninsula Group? *Antarctic Science*, *8*(4), 407–414.
- Hill, J. C., Gayes, P. T., Driscoll, N. W., Johnstone, E. A., & Sedberry, G. R. (2008). Iceberg scours along the southern US Atlantic margin. *Geology*, *36*(6), 447–450.
- Hodell, D. A., Kanfoush, S. L., Shemesh, A., Crosta, X., Charles, C. D., & Guilderson, T. P. (2001). Abrupt cooling of antarctic surface waters and sea ice expansion in the South Atlantic sector of the Southern Ocean at 5000 Cal Yr B.P. *Quaternary Research*, *56*(2), 191–198.
- Hodgson, D. A., Graham, A. G., Roberts, S. J., Bentley, M. J., Cofaigh, C. O., Verleyen, E., et al. (2014). Terrestrial and submarine evidence for the extent and timing of the Last Glacial Maximum and the onset of deglaciation on the maritime-Antarctic and sub-Antarctic islands. *Quaternary Science Reviews*, *100*, 137–158.
- Hulton, N. R., Purves, R. S., McCulloch, R. D., Sugden, D. E., & Bentley, M. J. (2002). The Last Glacial Maximum and deglaciation in southern South America. *Quaternary Science Reviews*, *21*(1–3), 233–241.
- Ineson, J. R., Crame, J. A., & Thomson, M. R. A. (1986). Lithostratigraphy of the Cretaceous strata of west James Ross Island, Antarctica. *Cretaceous Research*, *7*(2), 141–159.
- Isla, F. I., & Schnack, E. J. (1995). Submerged moraines offshore northern Tierra del Fuego, Argentina. In J. Rabassa, & M. Salemme (Eds.), *Quaternary of South America and Antarctica Peninsula* (Vol. 9, pp. 205–222). Rotterdam: A.A. Balkema.

- Ivanova, E. V., Murdmaa, I. O., Borisov, D. G., Simagin, N. V., Ovspeyan, E. A., et al. (2018). Geological and geophysical investigation of contourite systems from the Central and Southern Atlantic during Cruise 52 of the R/V Akademik Ioffe. *Oceanology*, 58(2), 322–324.
- Kasten, S., Schwenk, T., Aromokeye, D. A., Baques, M., Baumann, K. H., Bergenthal, M., et al. (2019). Dynamics of sedimentation processes and their impact on biogeochemical reactions on the continental slope off Argentina and Uruguay (MARUM) Cruise No. SO260/Leg 1 & Leg 2. *SONNE-Berichte*, 195. [https://doi.org/10.2312/cr\\_so260](https://doi.org/10.2312/cr_so260)
- Keany, J., Ledbetter, M. T., Watkins, N. D., & Huang, T.-C. (1976). Diachronous deposition of ice-rafted debris in sub-Antarctic deep-sea sediments. *Geological Society of America Bulletin*, 84, 2043–2053.
- Krastel, S., Wefer, G., Hanebuth, T. J., Antobreh, A. A., Freudenthal, T., Preu, B., et al. (2011). Sediment dynamics and geohazards off Uruguay and the de la Plata River region (northern Argentina and Uruguay). *Geo-Marine Letters*, 31(4), 271–283.
- La Nación (2002). Un témpano llegó a la altura de Mar del Plata. Retrieved from <https://www.lanacion.com.ar/sociedad/un-timpano-llego-a-la-altura-de-mar-del-plata-nid451697>
- Licht, K. J., & Hemming, S. R. (2017). Analysis of Antarctic glacial sediment provenance through geochemical and petrologic applications. *Quaternary Science Reviews*, 164, 1–24.
- Lim, A., Wheeler, A. J., & Arnaubec, A. (2017). High-resolution facies zonation within a cold-water coral mound: The case of the Piddington Mound, Porcupine Seamount, NE Atlantic. *Marine Geology*, 390, 120–130.
- Lonardi, A. G., & Ewing, M. (1971). Sediment transport and distribution in the Argentine Basin. 4. Bathymetry of the continental margin, Argentine Basin and other related provinces. Canyons and sources of sediments. *Physics and Chemistry of the Earth*, 8, 81–121.
- López-Martínez, J., Muñoz, A., Dowdeswell, J. A., Linés, C., & Acosta, J. (2011). Relict sea-floor ploughmarks record deep-keeled Antarctic icebergs to 45°S on the Argentine margin. *Marine Geology*, 288, 43–48.
- Mackintosh, A. N., Golledge, N., Domack, E., Dunbar, R., White, D., Pollard, D., McKay, R., et al. (2011). Retreat of the East Antarctic ice sheet during the last glacial termination. *Nature Geoscience*, 4, 195–202.
- Mackintosh, A. N., Verleyen, E., O'Brien, P. E., White, D. A., Jones, R. S., McKay, R., et al. (2014). Retreat history of the East Antarctic Ice Sheet since the last glacial maximum. *Quaternary Science Reviews*, 100, 10–30.
- Martínez, O., Rabassa, J., & Coronato, A. (2009). Charles Darwin and the first scientific observations on the Patagonian shingle formation (Rodados Patagónicos). *Revista de la Asociación Geológica Argentina*, 64, 90–100.
- Masson, D. G., Wynn, R. B., & Bett, B. J. (2004). Sedimentary environment of the Faroe-Shetland and Faroe Bank Channels, north-east Atlantic, and the use of bedforms as indicators of bottom current velocity in the deep ocean. *Sedimentology*, 51, 1207–1241.
- Matano, R. P., Palma, E. D., & Piola, A. R. (2010). The influence of the Brazil and Malvinas currents on the Southwestern Atlantic shelf circulation. *Ocean Science*, 6(4), 983–995. <https://doi.org/10.5194/os-6-983-2010>
- McCave, I. N. (2008). Size sorting during transport and deposition of fine sediments: sortable silt and flow speed. In M. Rebesco, A. Camerlenghi, & A. J. Van Loon (Eds.), *Contourite research: A field in full development. Developments in sedimentology* (Vol. 60, pp. 121–142). Elsevier.
- Mercer, J. H. (1976). Glacial history of southernmost South America. *Quaternary Research*, 6, 125–166.
- Mukasa, S. B., & Dalziel, I. W. (1996). Southernmost Andes and South Georgia Island, North Scotia Ridge: Zircon U-Pb and muscovite <sup>40</sup>Ar/<sup>39</sup>Ar age constraints on tectonic evolution of Southwestern Gondwanaland. *Journal of South American Earth Sciences*, 9(5–6), 349–365.
- Noble, T. L., Piotrowski, A. M., Robinson, L. F., McManus, J. F., Hillenbrand, C. D., & Bory, A. J. M. (2012). Greater supply of Patagonian-sourced detritus and transport by the ACC to the Atlantic sector of the Southern Ocean during the last glacial period. *Earth and Planetary Science Letters*, 317, 374–385.
- Orsi, A. H., Whitworth, T., III, & Nowlin, W. D., Jr (1995). On the meridional extent and fronts of the Antarctic Circumpolar Current. *Deep-Sea Research I*, 42(5), 641–673.
- Piola, A. R., & Gordon, A. L. (1989). Intermediate waters in the southwest South Atlantic. *Deep-Sea Research Part A. Oceanographic Research Papers*, 36(1), 1–16.
- Plafker, G., Bartsch-Winkler, S., & Ovenshine, A. T. (1977). Paleoglacial implications of coarse detritus in DSDP Leg 36 cores. In P. F. Barker, I. W. D. Dalziel, M. G. Dinkelman, D. H. Elliot, A. M. Gombos Jr, A. Lonardi, et al. (Eds.), *Initial Reports of the deep sea drilling project* (Vol. 36, pp. 857–864). Washington, DC: U.S. Government Printing Office. <https://doi.org/10.2973/dsdp.proc.36.119.1977>
- Preu, B., Hernández-Molina, F. J., Violante, R., Piola, A. R., Paterlini, C. M., Schwenk, T., & Spiess, V. (2013). Morphosedimentary and hydrographic features of the northern Argentine margin: The interplay between erosive, depositional and gravitational processes and its conceptual implications. *Deep-Sea Research Part I Oceanographic Research Papers*, 75, 157–174.
- Rabassa, J., & Clapperton, C. M. (1990). Quaternary glaciations of the Southern Andes. *Quaternary Science Reviews*, 9, 153–174.
- Rabassa, J., Coronato, A. M., & Salemme, M. (2005). Chronology of the Late Cenozoic Patagonian glaciations and their correlation with biostratigraphic units of the Pampean region (Argentina). *Journal of South American Earth Sciences*, 20(1–2), 81–103.
- Rackow, T., Wesche, C., Timmermann, R., Hellmer, H. H., Juricke, S., & Jungm, T. (2017). A simulation of small to giant Antarctic iceberg evolution: Differential impact on climatology estimates. *Journal of Geophysical Research: Oceans*, 122, 3170–3190. <https://doi.org/10.1002/2016JC012513>
- Rinaldi, C. A., Massabie, A., Morelli, J., Rosenmall, H. L., & Del Valle, R. (1978). In: *Geología de la Isla Vicecomodoro Marambio* (Vol. 217, p. 137). Buenos Aires, Argentina: Contribuciones del Instituto Antártico Argentino.
- Schodlok, M. P., Hellmer, H. H., Rohardt, G., & Fahrbach, E. (2006). Weddell Sea iceberg drift: Five years of observations. *Journal of Geophysical Research*, 111(C6), C06018. <https://doi.org/10.1029/2004JC002661>
- SHN Chart H5011 (2002). *Océano Atlántico Sudoccidental – desde el Rio de la Plata hasta el Mar de Weddell, 1a Edición*. Buenos Aires, Argentina: Servicio de Hidrografía Naval.
- Steinmann, L., Baques, M., Wenau, S., Schwenk, T., Spiess, V., Piola, A. R., et al. (2020). Discovery of a giant cold-water coral mound province along the northern Argentine margin and its link to the regional Contourite Depositional System and oceanographic setting. *Marine Geology*, 106223. <https://doi.org/10.1016/j.margeo.2020.106223>
- Stern, C. R., & De Wit, M. J. (2003). Rocas Verdes ophiolites, southernmost South America: remnants of progressive stages of development of oceanic-type crust in a continental margin back-arc basin. In Y. Dilek, & P. T. Robinson (Eds.), *Ophiolites in Earth history* (Vol. 218, pp. 665–683). London, UK: The Geological Society of London, Special Publications.
- Stuart, K. M., & Long, D. G. (2011). Tracking large tabular icebergs using the SeaWinds Ku-band microwave scatterometer. *Deep Sea Research Part II: Topical Studies in Oceanography*, 58(11–12), 1285–1300.
- Teitler, L., Warnke, D. A., Venz, K. A., Hodell, D. A., Becquey, S., Gersonde, R., & Teitler, W. (2010). Determination of Antarctic Ice Sheet stability over the last 500 ka through a study of iceberg-rafted debris. *Paleoceanography*, 25, PA1202. <https://doi.org/10.1029/2008PA001691>

- Tournadre, J., Bouhier, N., Girard-Arduin, F., & Rémy, F. (2016). Antarctic icebergs distributions 1992–2014. *Journal of Geophysical Research: Oceans*, *121*(1), 327–349. <https://doi.org/10.1002/2015JC011178>
- Tournadre, J., Girard-Arduin, F., & Legrésy, B. (2012). Antarctic icebergs distributions, 2002–2010. *Journal of Geophysical Research*, *117*, C05004. <https://doi.org/10.1029/2011JC007441>
- Tsuchiya, M., Talley, L. D., & McCartney, M. S. (1994). Water-mass distributions in the western South Atlantic; A section from South Georgia Island (54°S) northward across the equator. *Journal of Marine Research*, *52*, 55–81.
- Violante, R. A., Cavallotto, J. L., Bozzano, G., & Spoltore, D. V. (2017). Sedimentación marina profunda en el margen Continental Argentino: revisión y estado del conocimiento. *Latin American Journal of Sedimentology and Basin Analysis*, *24*(1), 7–29.
- Violante, R. A., Paterlini, C. M., Costa, I. P., Hernández-Molina, F. J., Segovia, L. M., Cavallotto, J. L., et al. (2010). Sismoestratigrafía y evolución geomorfológica del talud continental adyacente al litoral del este bonaerense, Argentina. *Latin American Journal of Sedimentology and Basin Analysis*, *17*(1), 33–62.
- Warratz, G., Schwenk, T., Voigt, I., Bozzano, G., Henrich, R., Violante, R., & Lantzsich, H. (2019). Interaction of a deep-sea current with a blind submarine canyon (Mar del Plata Canyon, Argentina). *Marine Geology*, *417*, 106002. <https://doi.org/10.1016/j.margeo.2019.106002>
- Watkins, N. D., Keany, J., Ledbetter, M. T., & Huang, T.-C. (1974). Antarctic glacial history from analyses of ice-rafted deposits in marine sediments: new model and initial tests. *Science*, *186*, 533–536.
- Weber, M. E., Clark, P. U., Kuhn, G., Timmermann, A., Spreng, D., Gladstone, R., et al. (2014). Millennial-scale variability in Antarctic ice-sheet discharge during the last deglaciation. *Nature*, *510*, 134–138.
- Weber, M. E., Raymo, M. E., Peck, V. L., & Williams, T. (2018). Expedition 382 Scientific Prospectus: Iceberg Alley and South Falkland Slope Ice and Ocean Dynamics. *International Ocean Discovery Program*, ISSN: 2332-1385, *382*, 56. <https://doi.org/10.14379/iodp.sp.382.2018>
- Wefing, A.-M., Arps, J., Blaser, P., Wienberg, C., Hebbeln, D., & Frank, N. (2017). High precision U-series dating of scleractinian cold-water corals using an automated chromatographic U and Th extraction. *Chemical Geology*, *475*, 140–148.
- Wentworth, C. K. (1936). An analysis of the shapes of glacial cobbles. *Journal of Sedimentary Petrology*, *6*(2), 85–96.
- Williams, T., van de Flierdt, T., Hemming, S. R., Chung, E., Roy, M., & Goldstein, S. L. (2010). Evidence for iceberg armadas from East Antarctica in the Southern Ocean during the late Miocene and early Pliocene. *Earth and Planetary Science Letters*, *290*(3–4), 351–361.
- Ziegler, A. F., Smith, C. R., Edwards, K. F., & Vernet, M. (2017). Glacial dropstones: islands enhancing seafloor species richness of benthic megafauna in West Antarctic Peninsula fjords. *Marine Ecology Progress Series*, *583*, 1–14.